Different Ionic Selectivities for Connexins 26 and 32 Produce Rectifying Gap Junction Channels

Thomas M. Suchyna,* Johannes M. Nitsche,# Mark Chilton,§ Andrew L. Harris,¶ Richard D. Veenstra,§ and Bruce J. Nicholson*

*Department of Biological Sciences and #Department of Chemical Engineering, SUNY at Buffalo, Buffalo, New York 14260; §Department of Pharmacology, SUNY Health Science Center, Syracuse, New York 13210; and ¶Department of Biophysics, Johns Hopkins University, Baltimore, Maryland 21218 USA

ABSTRACT   The functional diversity of gap junction intercellular channels arising from the large number of connexin isoforms is significantly increased by heterotypic interactions between members of this family. This is particularly evident in the rectifying behavior of Cx26/Cx32 heterotypic channels (Barrio et al., 1991. *Proc. Natl. Acad. Sci. USA.* 88:8410–8414). The channel properties responsible for producing the rectifying current observed for Cx26/Cx32 heterotypic gap junction channels were determined in transfected mouse neuroblastoma 2A (N2A) cells. Transfectants revealed maximum unitary conductances (γ_j) of 135 pS for Cx26 and 53 pS for Cx32 homotypic channels in 120 mM KCl. Anionic substitution of glutamate for Cl indicated that Cx26 channels favored cations by 2.6:1, whereas Cx32 channels were relatively nonselective with respect to charge. In Cx26/Cx32 heterotypic cell pairs, the macroscopic fast rectification of the current-voltage relationship was fully explained at the single-channel level by a rectifying γ_j that increased by a factor of 2.9 as the transjunctional voltage (V_j) changed from -100 to $+100$ mV with the Cx26 cell as the positive pole. A model of electrodiffusion of ions through the gap junction pore based on Nernst-Planck equations for ion concentrations and the Poisson equation for the electrical potential within the junction is developed. Selectivity characteristics are ascribed to each hemichannel based on either pore features (treated as uniform along the length of the hemichannel) or entrance effects unique to each connexin. Both analytical GHK approximations and full numerical solutions predict rectifying characteristics for Cx32/Cx26 heterotypic channels, although not to the full extent seen empirically. The model predicts that asymmetries in the conductance/permeability properties of the hemichannels (also cast as Donnan potentials) will produce either an accumulation or a depletion of ions within the channel, depending on voltage polarity, that will result in rectification.

INTRODUCTION

Gap junction channels are expressed in nearly every mammalian tissue and mediate the direct exchange of ions and small metabolites between cells (Tsien and Weingart, 1976; Dunlap et al., 1987; Saez et al., 1989). Gap junction channels are formed from two hemichannels provided by the apposed cells. These hemichannels comprise subunits termed connexins, 13 of which have been identified in mammals alone (Yeager and Nicholson, 1996; Kumar and Gilula, 1996). Many homotypic channels (junctional channels composed of identical subunits) have been characterized with respect to their sensitivity to transjunctional voltage (V_j) and selectivity to permeant molecules. These channels show a wide range of gating sensitivities to V_j (reviewed in Nicholson et al., 1993; Bruzzone et al., 1996). Selectivity for permeants, which in most systems is likely to be a more physiologically relevant attribute, has been demonstrated for both ions (Veenstra, 1996) and larger dyes (Elfgang et al., 1995; Veenstra, 1996; Cao et al., 1998) to

vary over an order of magnitude among different homotypic channels. The expression of multiple connexins in mammalian tissues adds further complexity, as there is already evidence for the formation of gap junction channels that are both heterotypic (formed of two homogeneous hemichannels, each composed of a different connexin) and heteromeric (each hemichannel contains two or more connexins) (Barrio et al., 1991; Hennemann et al., 1992; White et al., 1992; Jiang and Goodenough, 1996; Brink et al., 1997; Bevans et al., 1988; Falk et al., 1997). This huge potential for diversity has increased interest in the properties of intercellular channels produced by the interaction between different connexin isoforms.

Connexin subunit expression and interactions in mammalian liver have been well characterized since the initial observation that two connexins (26 and 32) could coexist in the same junctional plaque (Nicholson et al., 1987; Traub et al., 1989; Zhang and Nicholson, 1994). Expression of Cx26 or Cx32 cRNAs in paired *Xenopus* oocytes produces homotypic gap junction channels having essentially symmetrical but distinct gating properties in response to V_j (Barrio et al., 1991). In contrast, asymmetrical Cx26/Cx32 oocyte pairs produce a rectifying instantaneous conductance (increasing as the Cx26 side becomes relatively positive) and slow voltage sensitive closure only when the Cx26 side is relatively positive. Initially, this current-voltage relationship did not appear to reflect the homotypic properties of the component hemichannels (Barrio et al., 1991). However, mu-

tagenesis studies using the *Xenopus* oocyte expression system have suggested that a difference in the polarity of voltage to which Cx26 and Cx32 hemichannels respond is responsible for the asymmetrical steady-state gating properties of the heterotypic channels (Verselis et al., 1994). In contrast, the nature of the rectifying initial current of the heterotypic Cx26/Cx32 gap junctions has not been addressed. Two mechanisms by which this could be achieved are rapid, voltage-dependent changes in channel open probability (i.e., gating) or voltage-dependent changes in the unitary conductance of each channel. The contribution of each mechanism could be distinguished through single-channel analyses, requiring smaller cells with low levels of intercellular channel expression.

Here, we first determine the unitary conductance (γ_j) for Cx26 and Cx32 homotypic channels expressed by transfection into communication-deficient (Reed et al., 1993) N2A cells that do not express endogenous connexin RNA (Veenstra and Brink, 1992). It is demonstrated that the voltage gating properties of these channels expressed in N2A cells are similar to their properties determined in *Xenopus* oocytes. Second, it is shown that heterotypic Cx26/Cx32 channels can form between these cells, and as demonstrated in Hela cells by Bukauskas et al. (1995), each channel duplicates the rectifying properties observed macroscopically in oocytes (Barrio et al., 1991).

We then proceed to investigate the channel properties that give rise to the rectifying behavior of heterotypic Cx26/Cx32 channels. Based on the size of a gap junction channel (which has an aqueous pore diameter of 1.0–1.5 nm, allowing the passage of molecules of up to 1000 Da; Flagg-Newton et al., 1981; Brink and Dewey, 1980; Schwarzmann et al., 1981; Makowski et al., 1984; Verselis and Brink, 1986; reviewed in Veenstra, 1996), it has generally been assumed that it would impose little selectivity on the movement of inorganic ions of differing charge. However, several reports suggest that connexins show weak selectivity on the basis of charge. By measuring junctional conductance changes in response to substitution of anions in the electrode solution, Veenstra et al. (Veenstra et al., 1994, 1995; Veenstra, 1996) demonstrated that rat Cx40, human Cx37, and chicken Cx43 and 45 form weakly cation-selective channels (a range of ~2:1 to 10:1 cation/anion selectivity) when expressed in mouse N2A cells. More recently, the cation/anion selectivities of rat Cx43 and Cx40 channels were directly determined to be ~8:1 (Wang and Veenstra, 1997; Beblo and Veenstra, 1997). In general these findings correlate with results from larger dyes, such as variants of fluorescein with different anionic charge distributions (Veenstra et al., 1995). Using more qualitative assessments of gap junction permeability to a larger variety of permeants, Elfgang et al. (1995) showed that, although several mouse connexins expressed in HeLa cells are all permeable to the negatively charged dye Lucifer yellow, Cx31 and Cx32 channels showed a reduced ability to pass positively charged dyes. A quantitative approach to measurement of dye transfer in both HeLa transfectants and *Xenopus* oo-

cytes by Cao et al. (1998) clearly established permeability differences between Cx32 channels that favored the passage of anionic Lucifer yellow, and Cx26 and Cx45 channels, which favored the passage of cationic 4′,6-diamino-2-phenylindole dihydrochloride. This supports earlier observations of Harris et al. (1992) demonstrating anion selectivity of Cx32 hemichannels.

In the current work, anionic substitution directly demonstrates that Cx26 and Cx32 channels have opposite ionic selectivities, with Cx26 favoring cations (~2.6:1), and Cx32 slightly favoring anions, consistent with the results of Cao et al. (1998). Furthermore, we have developed a novel modification of the Poisson-Nernst-Planck (PNP) model (derived by Chen et al. (1992) and Chen and Eisenberg (1993), and extended by Nonner and Eisenberg (1998); reviewed by Eisenberg (1996)) that describes ion flux through gap junctional pores under the influence of an electrical potential. Application of several variants of this model (both analytical approximations and numerical solutions) to the Cx26/Cx32 heterotypic case reveals that the basic rectifying properties of this channel, at least in part, derive simply from the in series connection of two channels of different ionic conductances and selectivities.

MATERIALS AND METHODS

Transfection and detection of RNA transcripts

Full-length cDNAs for Cx26 (2.4 kb; Zhang and Nicholson, 1994) and Cx32 (1.5 kb; Paul, 1986) were cloned into the *Eco*RI site of pSFFV-neo (Fulbridge et al., 1988) and subsequently transfected into wt N2A cells using lipofectin (Boehringer-Mannheim, IN). Cells that received plasmid DNA were selected for by the addition of 0.5 μg/μl Geneticin (Sigma, St. Louis, MO) to the medium, and the colonies picked were maintained in 0.25 μg/μl Geneticin. Approximately 24 μg of poly A+ RNA from wt and transfected N2A cells and rat liver tissue as a positive control were run on a 1% agarose glyoxal denaturing gel, blotted onto Hybond (Amersham, IL) membranes, and probed with a 728-bp fragment from the Cx26 coding region (bp 317–1045) or a 772-bp fragment from the Cx32 coding region (bp 76–848). Fragments were labeled with [^{32}P]dCTP by random priming to a specific activity of 1.5×10^{-5} dpm/μl. Prehybridization was performed by incubating blotted membranes under standard conditions (1% sodium dodecyl sulfate (SDS), 1 M NaCl, 10% dextran sulfate, and 100 μg/ml denatured salmon sperm DNA) in a seal-a-meal bag for 2 h at 65°C. Subsequently, enough denatured probe was added to the bag to make a concentration of 0.75 dpm/ml and was then allowed to hybridize for 20 h at 65°C. Washes were performed in 2$\times$ standard saline citrate and 1% SDS at room temperature. Two clonal lines, Cx26#7 and Cx32#6, were chosen from the available pool of transfectants on the basis of cRNA expression levels and the presence of junctional coupling determined electrophysiologically.

Identification of heterotypic Cx26/Cx32 cell pairs

Cx26#7 and Cx32#6 N2A cell clones were grown in minimum essential medium containing 10% fetal bovine serum, 500 units/liter penicillin, and 0.5 mg/liter streptomycin. Cx32#6 cells were incubated for 10 min in medium containing 4 μM PKH2 fluorescent cell linker (Sigma) (Horan et al., 1990) and washed several times with fresh medium before harvesting by trypsinization and coculturing with Cx26#7 cells. Cx26#7/Cx32#6 cell pairs were identified after 24 h in coculture under epifluorescent illumination (490-nm excitation filter, 515-nm barrier filter).

Electrophysiological analysis on oocytes

cRNA transcripts to Cx26 and Cx32 cDNAs inserted into the *Eco*RI site of the pGEM7z vector (Promega, WI) with attached 5′ and 3′ *Xenopus* β-globin untranslated regions (described in Barrio et al., 1991) were prepared using SP6 RNA polymerase (Promega). Eight nanograms of Cx26 cRNA or 4 ng of Cx32 cRNA was coinjected into stage V or VI *Xenopus* oocytes with 8 ng of a 27-base antisense oligonucleotide complementary to nucleotides 327–353 of the Xen. Cx38 coding region to eliminate contributions from endogenous coupling. Injected oocytes were incubated for 24–48 h before they were stripped of their vitelline envelopes and oocytes were manually paired with vegetal poles apposed. After a further 16–24 h, recordings were made using a dual-electrode voltage clamp (Physiologic Instruments, San Diego, CA) in each oocyte. Current and voltage electrodes with resistances of ∼1 MΩ were filled with a 2 M KCl solution. Current traces were recorded on VCR tape, digitized with an Instrutech VR-100 A-D converter, and analyzed on an IBM-compatible 386 computer using Easy Plot (Spiral Software, Brookline, MA).

Electrophysiological analysis on N2A cells

Electrophysiological analysis and recording solutions have previously been described (Veenstra and Brink, 1992; Veenstra et al., 1994). Briefly, junctional current ($I_j = -\Delta I_2$) between N2A cell pairs was recorded by the dual whole-cell voltage-clamp method (Spray et al., 1979), using two 120 mM KCl patch electrodes containing (in mM) 120 KCl, 15 CsCl, 10 tetraethylammoniumCl, 1 KH_2PO_4, 3 $MgCl_2\text{-}6H_2O$, 0.068 $CaCl_2\text{-}2H_2O$, 5 EGTA, 25 HEPES, 3 Na_2ATP, and 3 Na_2 creatine phosphate (pH 7.0). Kglutamate electrodes contained the same ionic constituents as above, with equimolar substitution of Kglutamate for KCl. Current traces were filtered at 100 Hz and digitized at 2 kHz, and all-points current amplitude histograms were compiled from the inverse of the current from cell 2 for each experiment and fitted with a probability density function (*solid line* in histograms of Figs. 2–4).

RESULTS

Determination of connexin expression and heterotypic pair formation

Cx26 and Cx32 cDNAs subcloned into the pSFFV-neo vector (Fulbridge et al., 1988) under the constitutive cytomegalovirus promoter were transfected, via lipofection, into N2A cells that have no detectable endogenous gap junctional coupling or connexin expression (Veenstra and Brink, 1992; Reed et al., 1993). Expression of appropriate transcripts in selected Cx26#7 and Cx32#6 clones is shown by Northern blot in Fig. 1, *A* (Cx26 probe) and *B* (Cx32 probe). The increase in size of the transcripts in the transfectant cell lanes over those in the control lanes is as expected from the addition of SV40 5′ and 3′ untranslated sequences. Junctional coupling, measured by dual whole-cell voltage clamp (Veenstra and Brink, 1992), was observed in >80% of cell pairs from the Cx26#7 and Cx32#6 cell lines, although the average intercellular conductances (Cx26#7 = 0.6 ± 1.1 nS and Cx32#6 = 11.3 ± 3.8 nS; see Fig. 2 legend) suggest low protein expression levels (on average 5–200 channels/pair). In contrast, untransfected N2A cell pairs show coupling <15% of the time. The coupling in these cells probably reflects incomplete cell division because intercellular currents were usually large and insensitive to voltage or heptanol treatment, and fluorescein isothiocyanate-dextran

was found to move between these cells (Veenstra et al., 1994). Cx26/Cx32 heterotypic channels could be studied by coculturing Cx26#7 and Cx32#6 cells, where the latter were marked by a fluorescent lipophilic dye PKH2 (Horan et al., 1990). Cell pairs containing a "dye-marked" and "non-dye-marked" cell were chosen for recordings (Fig. 1, *C* and *D*), yielding an average conductance of 4.2 ± 2.7 nS. The asymmetrical currents between these pairs further confirmed that the pairs were heterotypic.

Connexins expressed in different systems produce junctions with similar macroscopic gating properties

Junctional current recordings from homotypic pairings of either Cx26#7 or Cx32#6 displayed time-dependent current decays in response to increasing V_j of either polarity (Fig. 2, *A* and *B*). These closely resembled the corresponding current recordings in *Xenopus* oocytes (Fig. 2, *C* and *D*, respectively). This is quantitatively confirmed by comparing the Boltzmann constants describing the voltage-dependent decrease in conductance for Cx26 ($V_O = +86$ mV, $A = 0.14$) and Cx32 ($V_O = \pm52$ mV, $A = 0.064$) in N2A cells with those determined in oocytes ($V_O = +82$ mV, $A = 0.14$ for Cx26, and $V_O = +55$ mV, $A = 0.09$ for Cx32) (Barrio et al., 1991). Heterotypic Cx26#7/Cx32#6 cell pairs also showed currents (Fig. 2 *E*), which closely approximated those observed in oocytes (Fig. 2 *F*). The initial conductance rectifies, increasing as the Cx26 cell becomes relatively more positive with respect to the Cx32 cell (slopes of 0.0044 for N2A cells and 0.0055 V^{-1} for oocytes; Barrio et al., 1991). V_j-sensitive closure is also evident only when the Cx26 cell is made relatively positive and is described by Boltzmann constants similar to those observed in oocytes ($V_O = +75$ mV, $A = 0.1$ for N2A cells and $V_O = +73$ mV, $A = 0.14$ for oocytes). These data, taken together, strongly suggest that the Cx26#7 and Cx32#6 cell lines express exclusively the transfected connexins and that the properties of the channels formed are unaffected by the differences between an amphibian and a mammalian expression system.

Homotypic Cx26 and Cx32 channels show different ionic conductances and selectivities

Single-channel currents were measured from cells expressing low levels of coupling (usually one or two channels). Representative current records with single-channel events are shown accompanied by histograms from Cx26#7 (Fig. 3, *A* and *B*) and Cx32#6 (Fig. 3, *C* and *D*) cell pairs. The γ_j for Cx26 channels, determined from the slope conductance of the I_j-V_j plot (Fig. 3 *G*), was 135 pS with 120 mM KCl in both electrodes, whereas Cx32 formed channels with γ_j of 53 pS under comparable conditions (Fig. 3 *H*). In addition, Cx32 channels commonly enter subconductance states that occur more frequently as V_j increases (Fig. 3, *E* and *F*). The discrepancy between these results and those reported
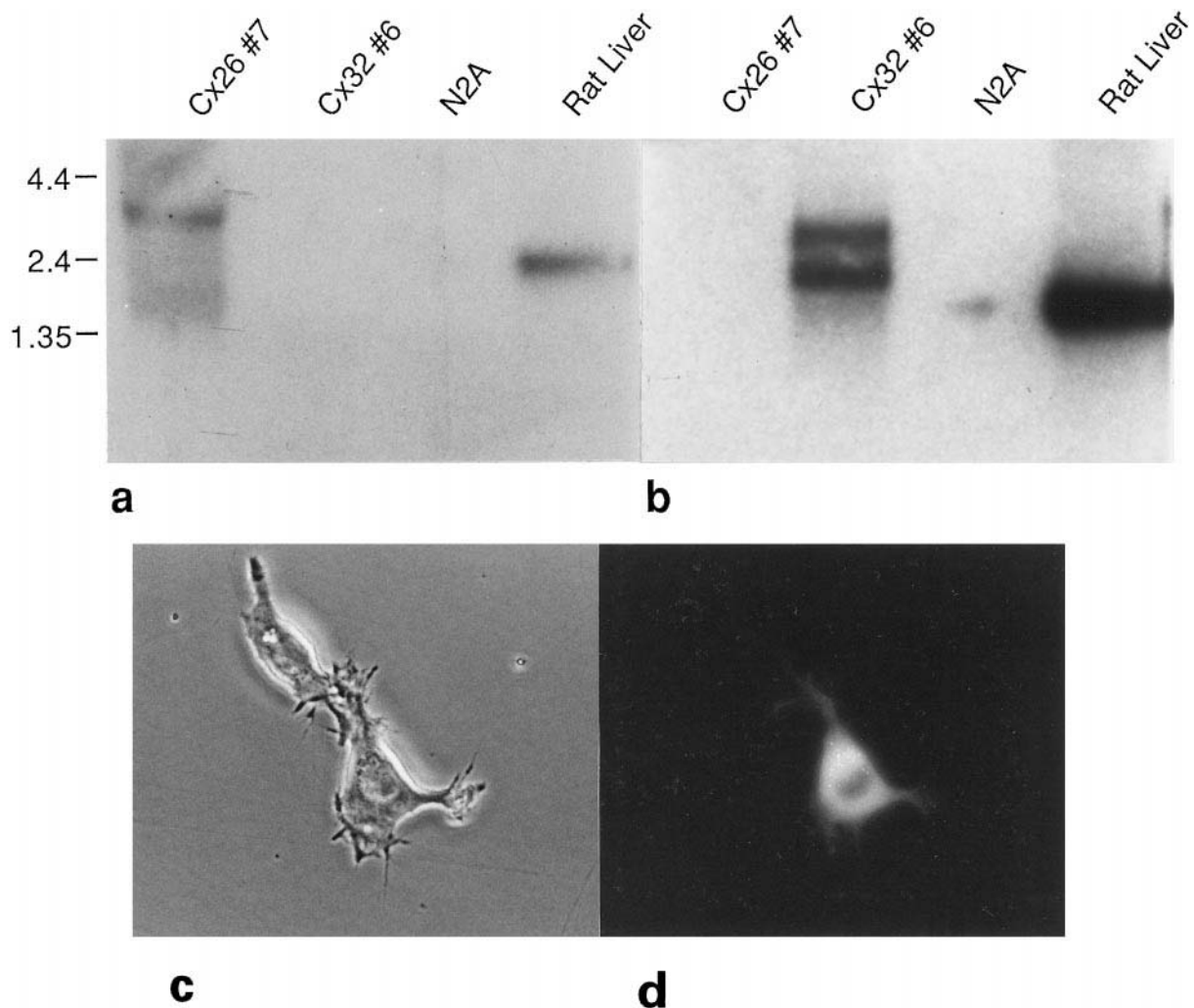
FIGURE 1   Northern blot analysis and heterotypic pair identification of N2A cell clones transfected with Cx26 and Cx32. (*A*) Cx26 probe recognizes specific bands in Cx26#7 (3.4 kb) and rat liver RNA (2.4 kb) lanes. (*B*) Stripped blot reprobed with Cx32 recognizes a 1.5-kb band in rat liver and a 2.7-kb/1.8-kb doublet in Cx32#7 lanes. The sizes of RNA bands in transfectants are ~1 kb larger because of the addition of SV40 3′ and 5′ noncoding regions. (*C*) Phase-contrast micrograph of a Cx26#7/Cx32#6 cell pair after 24 h in coculture, after prelabeling of the Cx32#6 cells with PKH2 fluorescent cell linker. (*D*) Epifluorescent illumination of the same cell pair allows identification of the two cell types.

previously for Cx32 in SKhep1 cells, where 120–130-pS channels were associated with Cx32 under similar conditions (Moreno et al., 1991), remains to be resolved. However, the same conductance value for both Cx26 and Cx32, as reported here, has now been reported for independently derived Hela transfectants by at least one other laboratory (Bukauskas et al., 1995).

Given the recent indications that different connexin channels may vary in their permeabilities to larger solutes (Elfgang et al., 1995; Steinberg et al., 1994; Moreno et al., 1991; Veenstra et al., 1995; Cao et al., 1998; Bevans et al., 1998), we also investigated the ion selectivity of Cx26 and Cx32 homotypic channels through a process analogous to that used for other ion channels (for a review see Hille, 1992). However, given the comparatively large size of junctional channels, we chose to substitute anions that were significantly different in size. Glutamate (~10 Å in length) has only one-fifth the aqueous mobility of Cl (~3.8 Å in

diameter unhydrated). Substitution of these anions in the electrode solution created significant differences in γ_j. These differences in γ_j could be used to define a relative anion/cation permeability ratio (R_p) of homotypic connexin channels, using the Goldman-Hodgkin-Katz (GHK) current equation (Eq. 13), modified such that the permeability of each anion is scaled by R_p (Veenstra et al., 1994). This empirical factor is equivalent to the channel anion/cation conductance ratio for an anion and cation pair with equal aqueous mobilities (Veenstra et al., 1995; Veenstra, 1996). Based on the assumption that the relative mobilities of ions within the channel are similar to those in bulk solution (Verselis and Brink, 1986), the following values of diffusion coefficients D_s were used (in units of 10^{-5} cm^2/s): 1.96 K$^+$, 2.06 Cs$^+$, 1.33 Na$^+$, 0.87 TEA$^+$, 2.03 Cl$^-$, and 0.387 glutamate$^-$ (Wang and Veenstra, 1997). For Cx26 channels, γ_j dropped from 135 pS to 112 pS with equimolar substitution of 120 mM Kglutamate for KCl in both electrodes
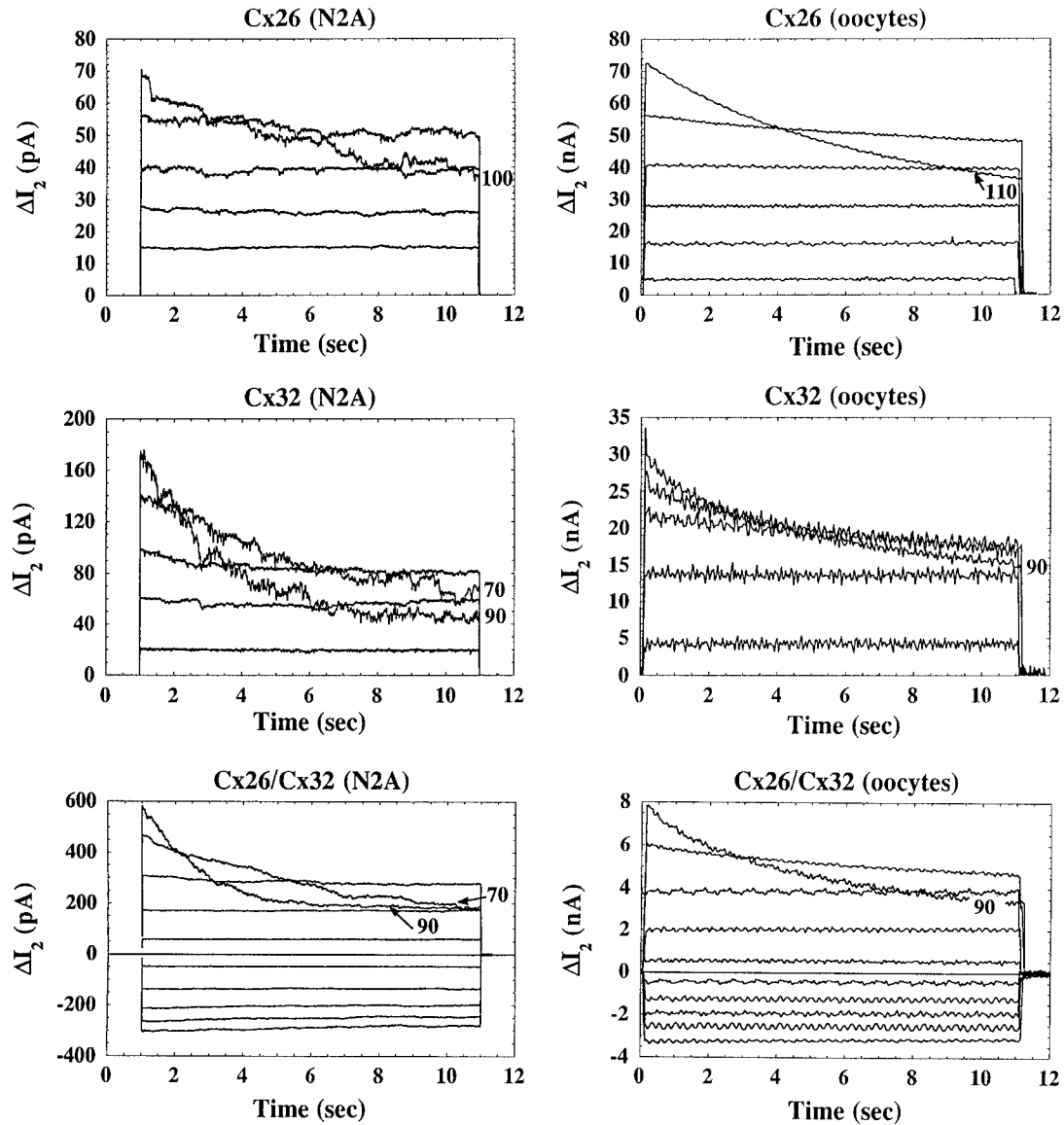
FIGURE 2 Comparison of the functional expression of homotypic Cx26 and Cx32, and heterotypic Cx26/Cx32 gap junctions in paired N2A cells and *Xenopus* oocytes shows that voltage gating of these channels in the two systems is identical. Junctional currents from N2A cell pairs (A, C, and E) display time- and V_j-dependent gating properties distinctly similar to their counterparts in *Xenopus* oocytes (B, D, and F, respectively). Average junctional conductances (g_j) from the transfected cell lines were Cx26#7 = 0.6 ± 1.1 nS (25/29, number of coupled pairs/total number of pairs tried); Cx32#6 = 11.3 ± 3.8 nS (81/98); heterotypic Cx26#7/Cx32#6 = 4.2 ± 2.7 nS (65/115). (A) Ensemble averages of the currents from nine V_j pulses of 20, 40, 60, 80, and 100 mV from a Cx26-transfected N2A cell pair containing four channels. (B) Junctional currents (I_j) from paired *Xenopus* oocytes injected with Cx26 cRNA in response to V_j steps of 10, 30, 50, 70, 90, and 110 mV. (C) Macroscopic I_j obtained from a Cx32-transfected N2A cell pair, with a g_j of 1.9 nS, subjected to V_j steps of 10, 30, 50, 70, and 90 mV. (D) I_j traces from paired *Xenopus* oocytes injected with Cx32 cRNA subjected to the same V_j steps as in C. (E) Macroscopic I_j traces from a Cx26#7/Cx32#6 heterotypic N2A cell pair (voltage steps applied to the Cx26 cell), with a g_j of 5.8 nS at +10 mV. Both positive and negative V_j steps of 10, 30, 50, 70, and 90 mV were applied. (F) I_j traces from pairings of Cx26 RNA and Cx32 RNA injected oocytes subjected to the same voltage steps as in E. Both show time- and V_j-dependent decay only for positive V_j steps and rectifying initial current.

(Fig. 3 G), from which an R_p of 0.38 was estimated. Equimolar KCl/Kglu substitution experiments for Cx32 reduced γ_j from 53 pS to 35 pS (Fig. 3 H), resulting in a calculated R_p of 1.06. Thus, in contrast to Cx26 channels that favor passage of cations, Cx32 channels are slightly more permeable to anions. We have also observed the same relative selectivity for charge for these two connexins, using larger fluorescent probes of opposite charge (Cao et al., 1998).

Heterotypic Cx26/C32 channels possess a rectifying unitary conductance

To better understand the mechanism underlying the rectifying instantaneous conductance of heterotypic Cx26/Cx32 channels, Cx26#7/Cx32#6 cell pairs that showed low intercellular conductance levels were selected for single-channel analysis. The channels recorded were unique in that the conductance of the main state did not have a unique value.
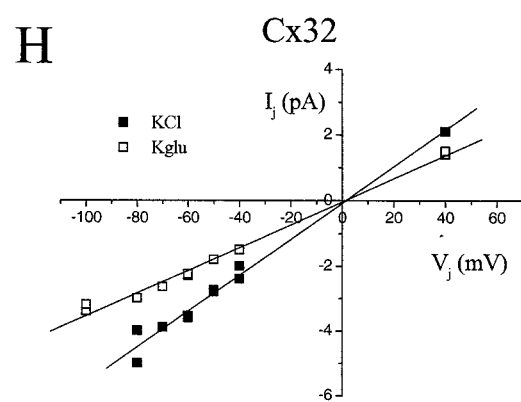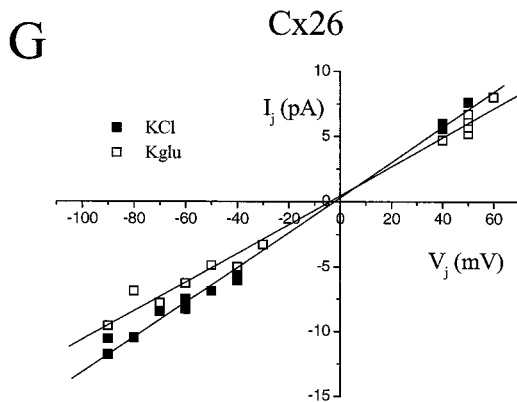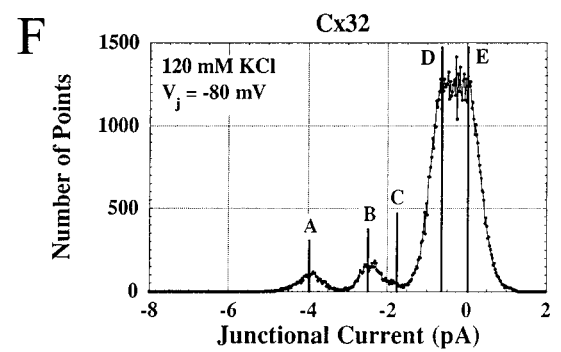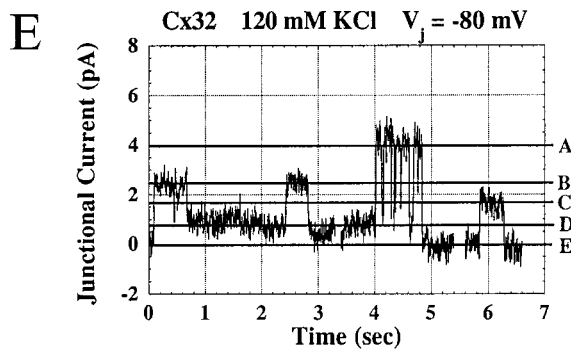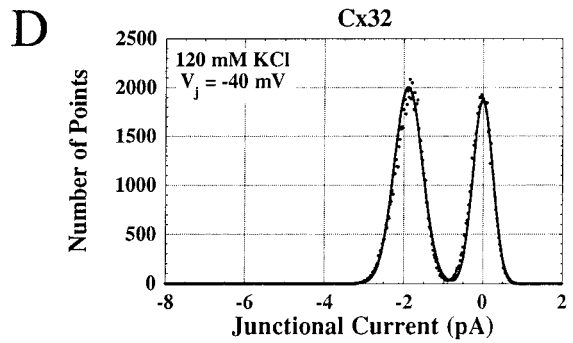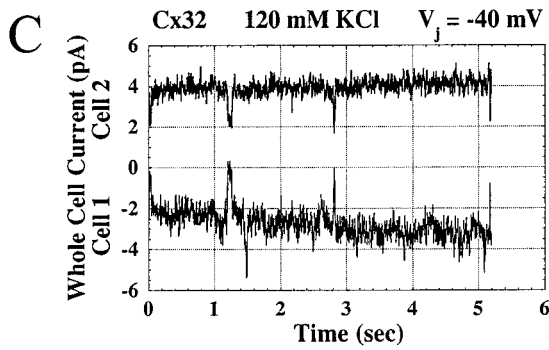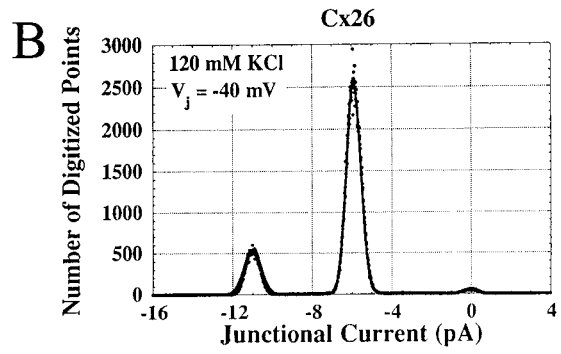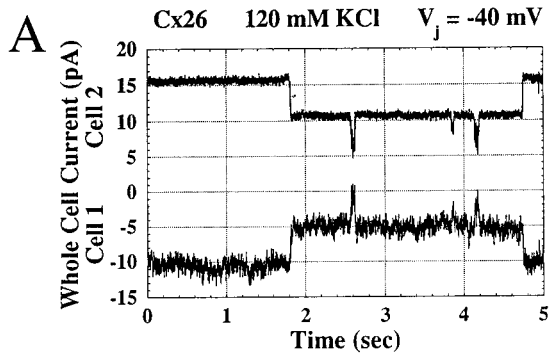
Rather, the γ_j increased as the applied voltage became progressively more positive with respect to the Cx26 cell (Fig. 4, A and B (positive), C and D (negative)). A plot of the single-channel currents (Fig. 4 E, *solid squares*) shows a parabolic increase with V_j that exactly coincides with the increases seen in macroscopic currents between either N2A cells (Fig. 4 E, *open squares*) or *Xenopus* oocytes (Fig. 4 E, *dotted line*) expressing Cx32/26 heterotypic channels.

Only positive V_j values greater than 60 mV with respect to the Cx26 cell produced a drop in channel P_o, consistent with the slow gating response seen at this polarity in the macroscopic records (data not shown). Thus the rectifying properties observed in the instantaneous macroscopic currents recorded in either oocytes or N2A cells are not due to changes in channel open probability (gating response), but are accounted for fully by changes in γ_j. In addition, at high positive voltages in the Cx26 cell (or negative voltages in the Cx32 cell), the slow gating response observed in the macroscopic currents is reflected in a decrease in P_o, which is superimposed on this single-channel rectifying behavior.

A transformation of these single-channel data to a plot of conductance (γ_j) as a function of V_j in both 120 mM KCl (Fig. 4 E, *solid squares*) and Kglutamate (Fig. 4 E, *open squares*) produces linear relationships with slopes of 44 pS/100 mV and 29 pS/100 mV, respectively (Fig. 4 F). The γ_j values at $V_j = 0$ ($\gamma_j(0)$) were 89 pS for KCl and 45 pS for Kglutamate. A previous study of these same channels in HeLa cells, recorded in Kaspartate (dotted line from Bukauskas et al., 1995), yielded results almost identical to the Kglutamate data shown here. Furthermore, the normalized slope of the KCl plot (0.0052 V^{-1}) closely matches the plot of the macroscopic conductance of Cx32/26 channels between *Xenopus* oocytes (0.0055 V^{-1} in Barrio et al., 1991). The molecular mechanism behind this rectification remains in question and does not seem to be fully explained by shifts in voltage gating of the channels, as has been proposed previously (Bukauskas et al., 1995). The rapid rectification of this and some other gap junctions is unique among ion channels in that it occurs in an environment where the ionic conditions at either end of the channel are essentially equivalent. In some cases, gap junction rectifi-

cation has been explained by rapid gating of the channel (Jaslove and Brink, 1986). However, in the case of the Cx26/Cx32 channel, where no change in P_o is observed, a new model must be sought to explain the rectification in γ_j.

A pore-scale electromigration/diffusion model of Cx26/Cx32 rectification: general principles and derivation of the model

A semiquantitative explanation of the observed rectifying behavior of Cx26/Cx32 heterotypic channels can be obtained using a modification of the Chen and Eisenberg (1993) model. This represents a one-dimensional model of ion flux through a long pore, based on the Nernst-Planck equations for the cation and anion concentrations, and the Poisson equation for the electrical potential.

The two hemichannels are represented as homogeneous cylindrical pores of equal length L, (distinguished by a superscript h (= l or r for "left" or "right")) through which ion transport occurs as a radially homogeneous (therefore effectively one-dimensional) process in, say, the x direction. Each hemichannel, h, is characterized by a cross-sectional area A^h and by the values of partition coefficients K_s^h and diffusion coefficients D_s^h specifying the affinity of ionic species s for the pore and the mobility of ionic species s within the pore, respectively. In the absence of structural information on the gap junction channel, the pore is assumed to be devoid of longitudinal structure, so that the parameters A^h, K_s^h, and D_s^h are constant along the length of each, although their values can differ between the two hemichannels. Essentially, the model that is developed is of two independent membrane channels connected head to head.

In the absence of ion-ion interactions, mass conservation in the left and right hemichannels is expressed by the Nernst-Planck equations (Chen and Eisenberg, 1993; Levitt, 1991; Hille, 1992; Hodgkin and Katz, 1949; Goldman, 1943),

$$d I_s^l / dX = 0,$$

$$I_s^l = -z_s F A^l D_s^l [d C_s^l / dX + (z_s F / RT)(d\Psi^l / dX) C_s^l],$$

$$-L < x < 0, \quad (1a)$$

FIGURE 3 Unitary conductances of Cx26 and Cx32 channels expressed in N2A cells. Representative ~5-s current records (A, C, and E) show prejunctional (cell 1) and postjunctional (cell 2 = I_j) current taken from longer duration V_j steps (as indicated). Accompanying histograms are shown to the right of the corresponding current traces (B, D, and F), where the sign conventions have been reversed to maintain consistency with the convention for I-V plots established previously (see Veenstra et al., 1994, 1995). The unitary channel current obtained from a Cx26-transfected cell pair (A) and the accompanying histogram (B) illustrate all stable conductance states during a 2-min V_j step produced by a hyperpolarizing cell 1 to −40 mV from a common holding potential of 0 mV. There were two active channels in this cell pair with amplitudes of −5.9 pA (36 channel events, first peak) and −5.1 pA (47 channel events, second peak) with variances of 0.3 pA. These transitions correspond to conductances of 148 and 128 pS, respectively. Cx32-transfected N2A cells (C and D) show one stable conductance state produced by a 2-min V_j step to −40 mV with an amplitude of −2.09 pA and a variance of 0.38 pA (52 +10 pS; 35 channel events). Multiple conductance states for Cx32 are revealed at a V_j of −80 mV (E and F). Gaps in the current trace correspond to 13.5- and 12-s intervals, which were omitted from the continuous current recording. Four distinct stable current levels of 4.0, 2.5, 1.8, and 0.7 pA and the ground state are labeled A–E, respectively. During the first 40 s after the step to −80 mV, distinct transitions of 4.0, 3.3, and 1.8 pA are evident, corresponding to conductances of 50, 41, and 23 pS (F). There were a total of 22 events at level A and 34 events at levels B and C. Distinct transitions between levels D and E were not observed and are within the noise limitations of these recordings. Single-channel I_j-V_j relations from Cx26 (G) and Cx32 (H) homotypic N2A cell pairs exposed to either 120 mM KCl (■) or 120 mM Kglutamate (□) electrode solutions. Each point in the I_j-V_j plot represents an amplitude obtained from the histogram at each V_j, where only transitions to level A (see E) were included for Cx32 at higher V_j. The solid lines represent current levels predicted from model 2 (pore scale convection-diffusion) described in the text and the Appendix.
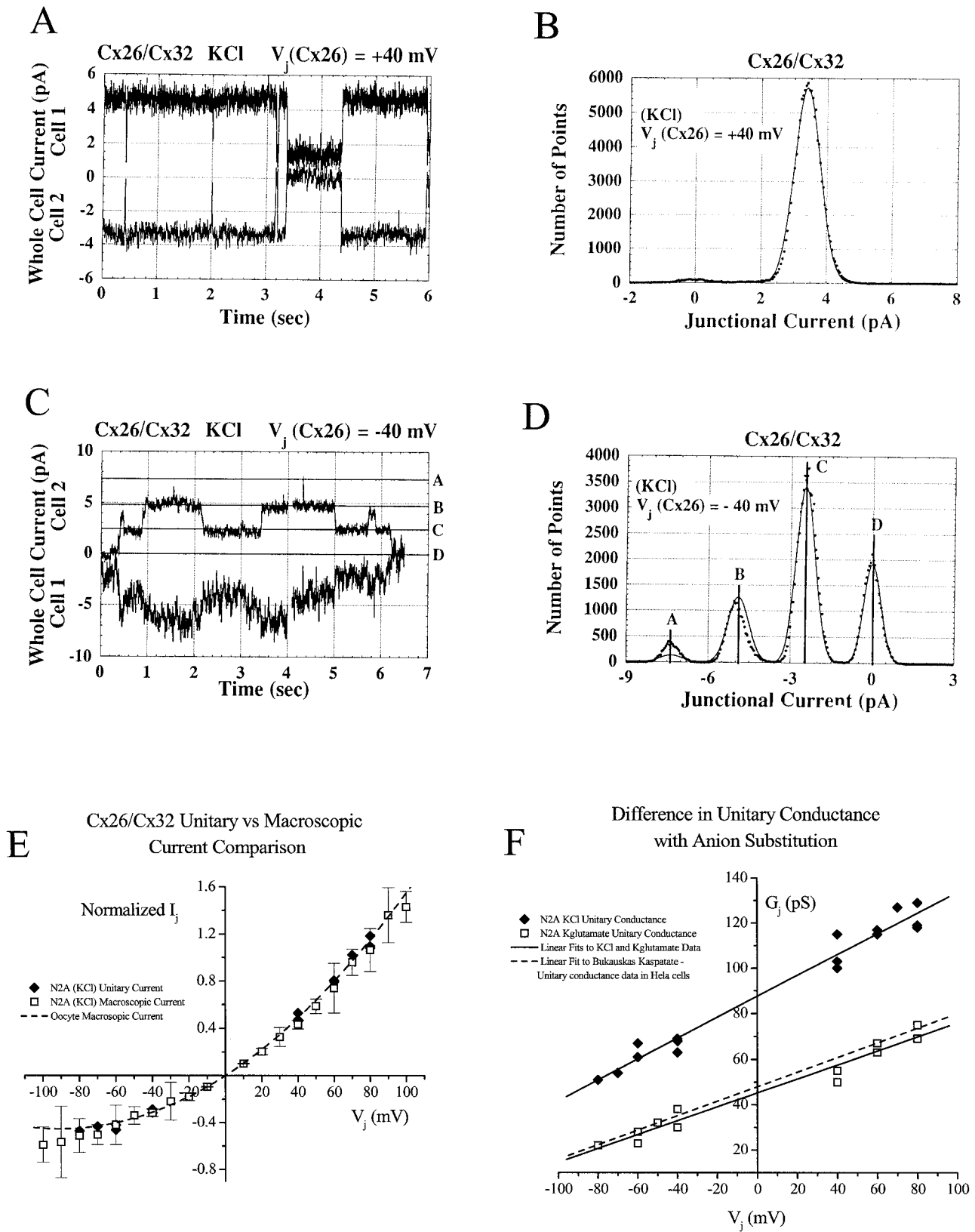
FIGURE 4 Unitary conductance and junctional current-voltage relationship of Cx26/Cx32 heterotypic channels. Representative current traces and histograms are presented as described in Fig. 3. (*A*) Unitary channel currents from a Cx26/Cx32 cell pair during a 2-min V_j step from 0 to +40 mV in the Cx26 cell reveal only one conductance state. The corresponding histogram (*B*), fitted with a probability density function, shows a current amplitude of 3.4 pA (59 channel events) with a variance of 0.4 pA. Channel currents from the same Cx26/Cx32 cell pair showed a distinctly different current level for the same size voltage step of opposite polarity (0 to −40 mV) in the Cx26 cell (*C*). With this opposite polarity V_j step, the three distinct current levels (*A–C*) observed in the 6-s record are apparent in the accompanying histogram (*D*), with amplitude levels separated by 2.45 pA and a variance of 0.24 pA. There

$$dI_s^r/dX = 0,$$

$$I_s^r = -z_s FA^r D_s^r [dC_s^r/dX + (z_s F/RT)(d\Psi^r/dX)C_s^r],$$

$$0 < x < L, \tag{1b}$$

cast in terms of the electrical currents I_s^h carried by ionic species s in hemichannel h. Each of these currents is the sum of a diffusive contribution arising from gradients in the ionic concentration $C_s^h(X)$ and a convective contribution representing electromigration driven by gradients in the electric potential $\Psi^h(X)$. Here, z_s denotes the valence of ionic species s, and F and R denote Faraday's constant and the universal gas constant, respectively. The electrical potential in each hemichannel is governed by the Poisson equation, in which the charge density arises from local deviations from electroneutrality of the solution in the pore:

$$d^2\Psi^l/dX^2 = -(F/\epsilon)\sum_s z_s C_s^l, \quad -L < x < 0,$$

and $\tag{2a,b}$

$$d^2\Psi^r/dX^2 = -(F/\epsilon)\sum_s z_s C_s^r, \quad 0 < x < L,$$

where ϵ is the dielectric constant of the fluid in the pore. While the contributions of the ions to the electrical field are accounted for here, no direct contributions of the pore lining to the potential are included in this one-dimensional model in the current absence of hard data on the pore structure. However, this can readily be incorporated. In fact, pore entrance effects (at the cytoplasmic entrance to each hemichannel) are accommodated in the current model by the introduction of an electrostatic surface potential E^h at the entrance of each hemichannel h. This can be attributed to either a local dipole or a fixed charge within the pore and hence is equivalent, in principle, to a Donan potential at the solution/pore interface. This induces ion concentrations to differ from the corresponding bulk values in the cell cytoplasm and is one possible means of conferring connexin-specific cation/anion selectivity (i.e., "selectivity filter"). In addition, partition coefficients K_s^h account for ionic affinities that are constant along the length of a hemichannel, although we will initially set these to unity.

These parameters establish boundary conditions for the PNP model, so that ion concentrations at the pore mouths are related to the bulk concentrations in the two cell interiors (assumed identical) by

$$C_s^l(-L) = K_s^l C_{\text{bulk-s}} \exp(-E^l z_s F/RT), \tag{3a}$$

$$C_s^r(L) = K_s^r C_{\text{bulk-s}} \exp(-E^r z_s F/RT), \tag{3b}$$

(Hille, 1992, p. 464; Frankenhaeuser, 1960). The electrical potential at each pore entrance is defined as

$$\Psi^l(-L) = \Delta V/2 + E^l, \quad \Psi^r(L) = -\Delta V/2 + E^r, \tag{4a,b}$$

where ΔV is the total drop in voltage across the cell pair from left to right.

By considering K_s^h as an equilibrium partition coefficient, mass transfer effects near the pore mouths are ignored, an assumption that has proved to be sound for long pores (although see Chen and Eisenberg (1993) for a discussion of this point). Ion selectivity arising from the Donnan surface potential E^h may also be expressed conveniently in terms of a Donnan ratio r_s^h. This will appear in subsequent equations and is defined as the concentration of ion s in the membrane pore ($C_s^h(\pm L)$) relative to bulk solution (as modified by any non-E^h-derived affinity ($K_s^h C_{\text{bulk-s}}$)), such that

$$r_s^h = \exp\left(\frac{-z_s E^h F}{RT}\right) = \frac{C_s^h(\pm L)}{K_s^h C_{\text{bulk-s}}}$$

$$= \sqrt{1 + \left(\frac{z_s \bar{X}}{2K_s^h C_{\text{bulk-s}}}\right)^2} - \frac{z_s \bar{X}}{2K_s^h C_{\text{bulk-s}}}, \tag{5}$$

where $\bar{X}$ represents a "fixed charge" within the pore, as defined in the original derivation of Teorell (1953). Details of the particular molecular structure that could produce this will have to await finer structural mapping of the pore.

There is also a need to impose certain conditions at the juncture of the two hemichannels. Hence, the left- and right-hand side currents for each species s must match and the electrostatic potential and its gradient must be continuous at the junction between the hemichannels, yielding

$$C_s^l(0)/K_s^l = C_s^r(0)/K_s^r, \quad I_s^l(0) = I_s^r(0), \tag{6a,b}$$

$$\Psi^l(0) = \Psi^r(0), \quad d\Psi^l/dX(0) = d\Psi^r/dX(0). \tag{7a,b}$$

were 4, 21, and 20 events for levels $A–C$, respectively. The normalized unitary current (◆) determined from histogram fits to 13 different V_j steps (2 min in duration) for two N2A cell pairs expressing low levels of Cx26/Cx32 channels are shown in E. These unitary current points exactly superimpose on the normalized macroscopic (multichannel) instantaneous current levels (□) for voltage steps between ±100 mV from four different N2A cell pairs (with standard error bars shown). The dashed line through the data points in E shows that the normalized macroscopic instantaneous currents in *Xenopus* oocyte pairs expressing Cx26/Cx32 heterotypic junctions also behave identically (data from Barrio et al., 1991). This illustrates that the macroscopic rectification of these channels seen in both oocytes and N2A cells is fully accounted for by the rectification of single channels. The single-channel conductance versus voltage data in the presence of 120 mM KCl (◆) or 120 mM Kglutamate (□) from Cx26/Cx32 heterotypic cell pairs is shown in F. Each set of data contains conductance values from two cell pairs. Linear regression fits to the conductance data (*solid lines*) show slope conductances and y intercepts of 0.46 pS/mV and 88 pS for KCl, and 0.31 pS/mV and 46 pS for Kglutamate. The dashed line through Kglutamate data is the linear regression fit (0.32 pS/mV slope conductance and 48 pS y intercept) through the unitary conductance data for Cx26/Cx32 channels expressed in Hela cells by Bukauskas et al. (1995), using Kaspartate as the charge carrier.

According to the preceding model, once the ionic concentration and electric potential have been solved for, the total current in the channels is calculable from

$$I = \sum_s I_s^l = \sum_s I_s^r. \tag{8}$$

The sum may be evaluated at any position X in either hemichannel because all of the individual ionic contributions I_s are independent of X (see Eqs. 1 and 6).

Our analysis focuses on the case where current is carried by a single monovalent salt, KCl. We identify potassium and chloride ions, respectively, with indices $s = 1$ and 2, and $z_1 = z_{K^+} = +1$, and $z_2 = z_{Cl^-} = -1$. Given these valencies, the respective Donnan ratios for hemichannel h are related by

$$r_{K^+}^h = \frac{1}{r_{Cl^-}^h} = \exp\left(\frac{-E^h F}{RT}\right). \tag{9}$$

Also,

$$C_{bulk-1} = C_{bulk-2} = C_{bulk}, \tag{10}$$

as required for electroneutrality of the bulk solution.

Analytical approaches—the constant-field assumption

The basic tenet underlying the classical Goldman-Hodgkin-Katz approach to Eqs. 1–4, 6, and 7 is that the electric field $d\Psi/dX$ is constant (or, equivalently, that the electric potential Ψ varies linearly with X) (Goldman, 1943; Hodgkin and Katz, 1949; Hille, 1992), an assumption that may or may not be consistent with the Poisson equation (Eq. 2). This assumption is removed below, but we adopt it for the moment because it turns out to be reasonably accurate for the purpose of fitting parameters, and because it leads to some useful qualitative insights.

With the constant-field assumption, the ion transport equation (Eq. 2) may be integrated analytically to yield the following well-known conclusion (Goldman, 1943; Hodgkin and Katz, 1949; Hille, 1992) used extensively below: if at positions X_α and X_β in hemichannel h the in-pore concentrations of ion s are $[S]_\alpha^h \equiv C_s^h(X_\alpha)$ and $[S]_\beta^h \equiv C_s^h(X_\beta)$ and the electric potential has the values $\Psi_\alpha^h \equiv \Psi^h(X_\alpha)$ and $\Psi_\beta^h \equiv \Psi^h(X_\beta)$, then the current I_s^h carried by ion s is given by

$$I_s^h = -\frac{z_s^2 F^2 A^h P_s^h}{RT} \frac{2L}{K_s^h} \frac{(\Psi_\beta^s - \Psi_\alpha^s)}{(X_\beta - X_\alpha)}$$

$$\frac{[S]_\beta^h - [S]_\alpha^h \exp[-(z_s F/RT)(\Psi_\beta^h - \Psi_\alpha^h)]}{1 - \exp[-(z_s F/RT)(\Psi_\beta^h - \Psi_\alpha^h)]}. \tag{11}$$

Here $2L$ is the total length of the channel, and $A^h P_s^h$ denotes the usual pore area-times-permeability factor for each ionic

species in each hemichannel, defined as

$$A^h P_s^h = A^h \frac{K_s^h D_s^h}{2L} \tag{12}$$

(Hodgkin and Katz, 1949; Hille, 1992).

Fitting of model parameters to homotypic channel conductance data and relative permeabilities

For a homotypic channel E^l and E^r are equal; hence the total in-pore voltage drop coincides with bulk (cytoplasm-to-cytoplasm) voltage drop ΔV. The total current I^h passing through such a pore (composed of two identical hemichannels of type h) is given by application of Eq. 12 with $X_\alpha = -L$, $X_\beta = L$, $[S]_\alpha^h = [S]_\beta^h = C_{bulk-s} K_s^h \exp(-z_s E^h F/RT)$, $\Psi_\alpha^h = \Delta V/2 + E^h$, and $\Psi_\beta^h = -\Delta V/2 + E^h$, which yields

$$I^h = \frac{F^2 C_{bulk}}{RT} \Delta V \sum_{s=1}^{2} z_s^2 A^h P_s^h \exp(-z_s E^h F/RT)$$

$$= \frac{F^2 C_{bulk}}{RT} \Delta V [A^h P_{K^+}^h \exp(-E^h F/RT) \tag{13}$$

$$+ A^h P_{Cl^-}^h \exp(+E^h F/RT)].$$

The exponential factors involving Ψ in Eq. 11 cancel out because of the equality of the left- and right-hand solution concentrations. It is now clear that conductance data can give a direct indication only of the lumped parameter $A^h P_{K^+}^h \exp(-E^h F/RT) + A^h P_{Cl^-}^h \exp(+E^h F/RT)$; the data for the homotypic Cx26 and Cx32 channels yield the numerical values 2.99×10^{-19} m^3/s and 1.18×10^{-19} m^3/s, respectively.

Our present estimates of relative permeabilities (R_p) apply only approximately to these equations for a number of reasons, the most important being that these equations account only for the dominant ions potassium and chloride. Slight differences in aqueous mobilities between potassium and chloride, and between bulk and internal pore solutions, are also neglected in this calculation. Nevertheless, the R_p values serve to approximate the relative amounts of current carried by cations and anions as follows:

$$\frac{A^{26} P_{Cl^-}^{26} \exp(-E^{26} F/RT)}{A^{26} P_{K^+}^{26} \exp(+E^{26} F/RT)} \cong R_p^{26} = 0.38, \tag{14}$$

$$\frac{A^{32} P_{Cl^-}^{32} \exp(-E^{32} F/RT)}{A^{32} P_{K^+}^{32} \exp(+E^{32} F/RT)} \cong R_p^{32} = 1.06. \tag{15}$$

These values constitute the essential link between model and experiments for homotypic channels, which forms the foundation for our theoretical consideration of heterotypic channels to follow.

Unique determination of the parameters requires precise knowledge of the physical origin of ionic selectivity, which at present we can only guess at. In the absence of informa-

tion, it is constructive to consider the two extreme cases where either 1) ionic selectivity arises solely from differences in the in-pore area-times-permeability factors, $A^h P_s^h$, and there is no surface potential ($E^h = 0$), or 2) ionic selectivity arises solely from the surface potential E^h at the hemichannel-cytoplasm interface, and the area-times-permeability factors are equal ($A^h P_{K^+}^h = A^h P_{Cl^-}^h$, but $A^{26} P_s^{26} \neq A^{32} P_s^{32}$). Using the perm-selectivity values for Cx26 and Cx32 derived above, these assumptions lead to the following two sets of parameter values consistent with the homotypic channel conductance data and relative permeabilities:

Case 1:

$$A^{26}P_{K^+}^{26} = 2.17 \times 10^{-19}\ \text{m}^3/\text{s}, \quad A^{32}P_{K^+}^{32} = 0.57 \times 10^{-19}\ \text{m}^3/\text{s},$$
$$A^{26}P_{Cl^-}^{26} = 0.82 \times 10^{-19}\ \text{m}^3/\text{s}, \quad A^{32}P_{Cl^-}^{32} = 0.61 \times 10^{-19}\ \text{m}^3/\text{s},$$
$$E^{26} = 0\ \text{mV}, \quad E^{32} = 0\ \text{mV},$$

(16)

Case 2:

$$A^{26}P_{K^+}^{26} = 1.34 \times 10^{-19}\ \text{m}^3/\text{s}, \quad A^{32}P_{K^+}^{32} = 0.59 \times 10^{-19}\ \text{m}^3/\text{s},$$
$$A^{26}P_{Cl^-}^{26} = 1.34 \times 10^{-19}\ \text{m}^3/\text{s}, \quad A^{32}P_{Cl^-}^{32} = 0.59 \times 10^{-19}\ \text{m}^3/\text{s},$$
$$E^{26} = -12.4\ \text{mV}, \quad E^{32} = +0.75\ \text{mV}.$$

(17)

The surface potentials given above are equivalent to the following Donnan ratios, as developed in Eq. 5 above:

Case 1:

$$r_{K^+}^{26} = 1/r_{Cl^-}^{26} = 1, \quad r_{K^+}^{32} = 1/r_{Cl^-}^{32} = 1,$$

(18)

Case 2:

$$r_{K^+}^{26} = 1/r_{Cl^-}^{26} = 1.62, \quad r_{K^+}^{32} = 1/r_{Cl^-}^{32} = 0.97.$$

(19)

Analytical theory for heterotypic channels

Equation 11 cannot be applied directly to the heterotypic Cx26/Cx32 channel because the permeability P_s is not a constant throughout the channel. We therefore apply this equation to the left and right hemichannels individually, using the symbol $[S]_{bulk} \equiv C_{bulk\text{-}s}$ to denote the bulk concentration of ions s (which is the same in the two cellular compartments, and the same for K^+ and Cl^- in this case). The two resulting GHK current equations,

$$I_s^l = \frac{z_s^2 F^2 A^l P_s^l}{RT} 2(\Delta\Psi)^l \frac{r_s^l [S]_{bulk} - \lfloor \acute{S} \rfloor_c \exp[-(z_s F/RT)(\Delta\Psi)^l]}{1 - \exp[-(z_s F/RT)(\Delta\Psi)^l]},$$

(20)

$$I_s^r = \frac{z_s^2 F^2 A^r P_s^r}{RT} 2(\Delta\Psi)^r \frac{\lfloor \acute{S} \rfloor_c - r_s^r [S]_{bulk} \exp[-(z_s F/RT)(\Delta\Psi)^r]}{1 - \exp[-(z_s F/RT)(\Delta\Psi)^r]},$$

(21)

contain a new unknown, namely the effective ionic concentration at the junction between hemichannels, $\lfloor \acute{S} \rfloor_c \equiv C_s^l(0)/K_s^l = C_s^r(0)/K_s^r$ (cf. Eq. 6a). Here $(\Delta\Psi)^l$ and $(\Delta\Psi)^r$ denote the

voltage drops within the left and right hemichannels, which are also unknown individually, although they must sum to the total drop in in-pore potential across the channel:

$$(\Delta\Psi)^l + (\Delta\Psi)^r = (\Delta\Psi)^{tot} = \Delta V + E^l - E^r.$$

(22)

In terms of $(\Delta\Psi)^l$ and $(\Delta\Psi)^r$, the concentration $\lfloor \acute{S} \rfloor_c$ at the junction between hemichannels can be determined from the requirement that the left- and right-hand currents match, i.e.,

$$I_s^l = I_s^r$$

(23)

(cf. Eq. 6b). The combination of Eqs. 20 and 21 according to the equalities expressed in Eqs. 22 and 23 tacitly assumes that ions occupying the center in-pore "compartment" at the junction between the hemichannels obey the principles of ionic independence (i.e., K^+ only influences K^+, etc.). This infers that ions entering from the right and left hemichannels mix in the center compartment and are influenced only by their electrochemical potentials relative to bulk solution. At present, we do not have any knowledge of what ion-ion and ion-site interactions occur at the hemichannel junction nor of its molecular composition. We find

$$\frac{[\acute{S}]_c}{[S]_{bulk}}$$

$$= \frac{\begin{aligned}&A^l P_s^l (\Delta\Psi)^l r_s^l - A^r P_s^r (\Delta\Psi)^r r_s^r \exp[-(z_s F/RT)(\Delta\Psi)^{tot}]\\ &- [A^l P_s^l (\Delta\Psi)^l r_s^l - A^r P_s^r (\Delta\Psi)^r r_s^r]\exp[-(z_s F/RT)(\Delta\Psi)^r]\end{aligned}}{\begin{aligned}&A^r P_s^r (\Delta\Psi)^r - A^l P_s^l (\Delta\Psi)^l \exp[-(z_s F/RT)(\Delta\Psi)^{tot}]\\ &- [A^r P_s^r (\Delta\Psi)^r - A^l P_s^l (\Delta\Psi)^l]\exp[-(z_s F/RT)(\Delta\Psi)^l]\end{aligned}},$$

(24a)

which reduces to

$$\frac{[\acute{S}]_c}{[S]_{bulk}} = \frac{A^l P_s^l r_s^l + A^r P_s^r r_s^r \exp[-(z_s F/RT)(\Delta\Psi)^{tot}/2]}{A^r P_s^r + A^l P_s^l \exp[-(z_s F/RT)(\Delta\Psi)^{tot}/2]}$$

(24b)

when $(\Delta\Psi)^l = (\Delta\Psi)^r$.

This result makes it possible to calculate the total current, using Eq. 8 together with either Eq. 20 or Eq. 21, provided we know how much of the total in-pore voltage drop occurs in each of the left and right hemichannels.

Calculations not shown indicate that the relative values of $(\Delta\Psi)^l$ and $(\Delta\Psi)^r$ do not strongly affect the current. Thus the results presented here are based on the assumption that $(\Delta\Psi)^l = (\Delta\Psi)^r$. Fig. 5 A shows the predicted current-voltage characteristics for cases 1 and 2, which have the correct qualitative behavior (i.e., greater conductance when the Cx26 side is positive relative to the Cx32 side), although the degree of rectification seen empirically is not fully accounted for. This is equally true for both cases 1 and 2, so it is impossible to distinguish between the possible mechanisms for ionic selectivity (differences in permeability and/or the existence of surface potentials) with this approach. In this regard it is worth noting that pore cross-sectional area A^h, the ionic diffusivities D_s^h, and the partition coefficients K_s^h occur only in the combination $A^h P_s^h$ in the

Analytical Fit to Cx26/Cx32 Single Channel Currents
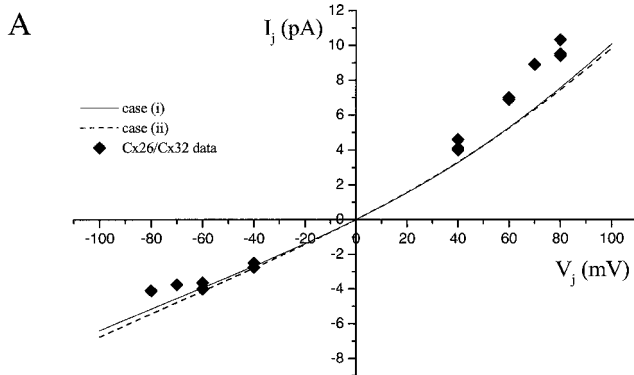
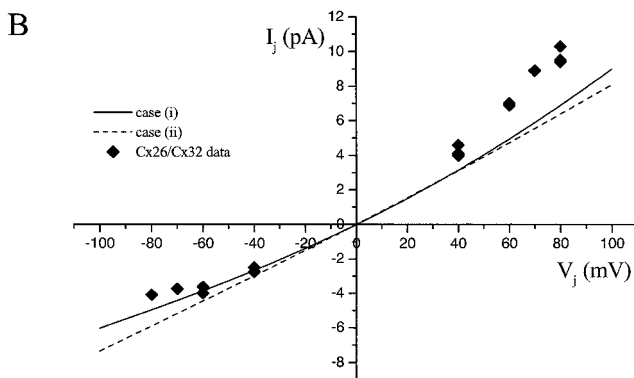## Numerical Fit to Cx26/Cx32 Single Channel Currents

FIGURE 5   (A) Current-voltage characteristics resulting from the analytical solution for Cx26/Cx32 heterotypic channels (based on Eq. 7 together with Eq. 22 or Eq. 23, assuming equal voltage drops in left (Cx26) and right (Cx32) hemichannels). The solid and dashed curves correspond to parameter values for cases 1 and 2, respectively, and are almost identical. Experimental points are included for comparison. (B) Current-voltage characteristics resulting from the complete numerical solution of the Nernst-Planck and Poisson equations for Cx26/32 heterotypic channels (see Appendix), with solid and dashed curves again corresponding to parameter values for cases 1 and 2, respectively. Experimental points are included for comparison. Case 1 shows more pronounced rectification than case 2. The reasons for an incomplete fitting of the data in any of the models is discussed in the text, and likely stems from the potential errors in the estimates of R_p (relative cation:anion preferences of the channels) and a simplistic view of the channel enforced by a lack of structural data.

final equations. Thus the present analytical theory also cannot distinguish between the possible mechanisms (pore size, mobility within the pore, partitioning) for the observed differences in conductance and selectivity of Cx32 and Cx26 homotypic channels.

This analytical solution to the heterotypic channel predicts that rectification is at least partially accounted for by differences in the ionic selectivities of the two hemichannels, attributed to either asymmetrical surface (or Donnan) potentials, ionic permeabilities within the pore, or a combination of these effects. However, this approach fails to account fully for the experimentally observed rectification (Fig. 5 A). It also does not completely account for the increase in current obtained in

KCl relative to Kglutamate (data not shown). This suggests that assigning the cation/anion selectivity entirely to differences in Cx26 and Cx32 electrostatic surface charges within the pore is likely to be an oversimplification.

The operative factor for equalizing the fluxes between the two hemichannels is the voltage-driven ionic concentration profiles in the center of the pore (the $[\acute{S}]_c$ term in Eqs. 20, 21, and 24), which cannot be demonstrated experimentally. Interpreted in terms of the "fixed charge theory" of Teorell (1953), both sides of the membrane would establish a permanent Donnan equilibrium such that the excess of cations (and reciprocal deficit of anions) on the Cx26 side exactly matches the net electrostatic potential across the channel. Furthermore, each hemichannel can be treated as a single "site" within the membrane that is always in equilibrium with the cytoplasmic bulk solution and the center (in-pore) "solution." This negates the need to assume inhomogeneities within the membrane, because any ion either exists in aqueous phase in one of the "compartments" or resides at a single "site" within the channel. No other structure has to be inferred regarding the location of the electrostatic potential and/or site within the membrane or the central compartment. It is only necessary that cation/anion independence at all locations is maintained. The data presented here do not directly address the issue of the existence of a "binding site" within the hemichannel, but it is common practice to assign the simplest state diagram of the ionic permeation process to a channel (i.e., single site, two barriers) for the purpose of subsequent experimentation.

Numerical theory for heterotypic channels— rationale and results

One limitation to the analytical solution presented above is that it assumes a constant field within the hemichannel, rather than deriving it from the Poisson equation (Eq. 2). However, this assumption would not be valid in the presence of any nonzero surface potentials or unequal partition coefficients that cause the concentrations of cations and anions to differ (see Chen et al., 1992). By assuming a Donnan equilibrium, as was done in the analytical derivation, this charge density is exactly compensated for by a fixed charge within the pore, thereby maintaining a linear field even in the presence of significantly different free cation and anion concentrations within the pore. If the fixed charge assumption is removed, the resulting nonuniform electric field, $d\Psi/dX$, would in turn cause the ionic concentrations to vary with position X. This would now require a numerical approach to solving Eqs. 1–4, 6, and 7 as they are coupled and nonlinear and inaccessible to exact analytical solution.

A finite-difference scheme developed to solve Eqs. 1–4, 6, and 7 is summarized in the Appendix. This numerical approach also predicts a local separation of charge, but in the absence of a compensatory charge in the pore it rapidly

decays (as a manifestation of the phenomenon that ionic concentrations relax to a condition of electroneutrality within a few Debye screening lengths of any charged surface or interface; see, e.g., Hiemenz, 1986, Chap. 12). Thus cationic and anionic concentrations become nearly equal over much of the pore (data not shown), resulting in significantly less charge separation between resident ions within the pore than is predicted by the analytical solution.

A result of this tendency toward electroneutrality is that the electric potential is roughly linear in the middle of the pore. The total concentration of charge carriers $C_{K^+}^h(X) + C_{Cl^-}^h(X)$ remains roughly constant throughout the pore. These two facts explain why the overall channel conductance predicted by the GHK equation can be quite insensitive to the predicted ion concentration profiles. Consistency between the numerical treatments of Eqs. 1–4, 6, and 7 with the empirical homotypic channel conductance data requires a modification of some of the area-times-permeability values for case 2. In particular, Eq. 17 must be amended as follows:

$$A^{26}P_{K^+}^{26} = A^{26}P_{Cl^-}^{26} = 1.51 \times 10^{-19} \text{ m}^3/\text{s.} \qquad (25)$$

Owing to the small surface potential and the small resulting ionic charge separation, case 2 area-times-permeability values for Cx32 hemichannels are correct to the number of digits exhibited.

Application of the finite-difference scheme (see Appendix) to a heterotypic Cx26/Cx32 channel yields the current-voltage characteristics shown in Fig. 5 B. As in the analytical case, the model describes a rectifying property for these heterotypic channels but falls short of predicting the full extent of the rectification. The consistent behavior of both analytical and numerical solutions in underestimating the degree of rectification observed empirically is likely to be the result of the inherently simple model of the pore that we are forced to use in the absence of better defined structural information on gap junctions. As discussed below, specific binding sites or point charges on the channel wall would significantly change the outcome of the model. Nonetheless, it is significant that such an inherently simple model can qualitatively account for the observed behavior. In the full numerical solution, case 1 parameters give a somewhat more pronounced current rectification than case 2, in better agreement with the data (Fig. 5 B), suggesting that selectivity is better explained by permeability factors than by surface potentials.

Ionic concentration profiles along the length of these heterotypic channels can be calculated from the numerical model for both case 1 (Fig. 6, A and B) and case 2 (Fig. 6, C and D) at transjunctional potentials of either polarity. Consistent with the better fit of case 1 to the data, these plots reveal a physically more reasonable picture of ion distribution involving significantly less separation of charge in this case. Examination of these ionic concentration profiles for case 1 (Fig. 6, A and B) suggests that a physical mechanism that contributes to heterotypic channel rectification may lie

in an accumulation (when the Cx26 cell is positive) or depletion (when the Cx32 cell is positive) of ions within the channel. This is discussed in detail below (also see Fig. 7).

DISCUSSION

The continuing characterization of more connexin isoforms has generated an increasing awareness of gap junctions as a family of diverse channels. To understand this diversity, recent studies have investigated the degree to which different connexins can interact and the effects of connexin composition on the permeability of the channels. Both heterotypic (between cells; Barrio et al., 1991; Hennemann et al., 1992; White et al., 1992, 1995; Elfgang et al., 1995) and heteromeric (within the same cell; Stauffer, 1995; Koval et al., 1995; Jiang and Goodenough, 1996) interactions between connexins have been reported. Extensive comparisons of heterotypic combinations reveal a complex pattern of allowed and disallowed connexin pairings (White et al., 1995; Yeager and Nicholson, 1996). Several of these pairings have yielded channels expressing novel properties not predicted from the parental homotypic forms.

Comparisons of gap junction permeability to both ions and large dyes have also revealed a marked dependence on connexin composition that includes differences in charge selectivity for both ions (Veenstra et al., 1994, 1995; Veenstra, 1996) and larger molecules (Elfgang et al., 1995; Veenstra et al., 1995; Bevans et al., 1998; Cao et al., 1998). Given the complex patterns of connexin expression in most tissues, it seems likely that these two aspects of junctional diversity are superimposed in many situations. This raises the prospect that hemichannels of different permeabilities could be connected in series, a unique situation among biological channels studied to date. In the current study, our examination of homotypic and heterotypic channels formed by Cx26 and Cx32 has provided evidence for differential ionic selectivity as the property of gap junction hemichannels that yields rectifying gap junction channels. This phenomenon has been observed in several combinations of different connexins with Cx32 (Barrio et al., 1991; White et al., 1995; Dahl et al., 1997). Using molecular modeling of the electrical and chemical gradients that arise from this "biological diode," we have described a mechanism that contributes significantly to this rectifying behavior.

Given the demonstrated coexpression of Cx32 and Cx26 in the same junctional structures of hepatocytes, the rectifying nature of heterotypic junctions between these connexins has always carried potential physiological significance. Cx32 and Cx26 homotypic channels showed characteristic and stable main states of 55 and 135 pS, respectively, with additional substrates evident in the former. Through anion exchange of glutamate for Cl$^-$ (see Veenstra et al., 1995, for a rigorous treatment), R_p values (ratios of cation to anion permeability when both are the same size) of 1.06 and 0.38 for Cx32 and Cx26 were established. The R_p model relies on the ratios of ionic aqueous mobilities to determine the

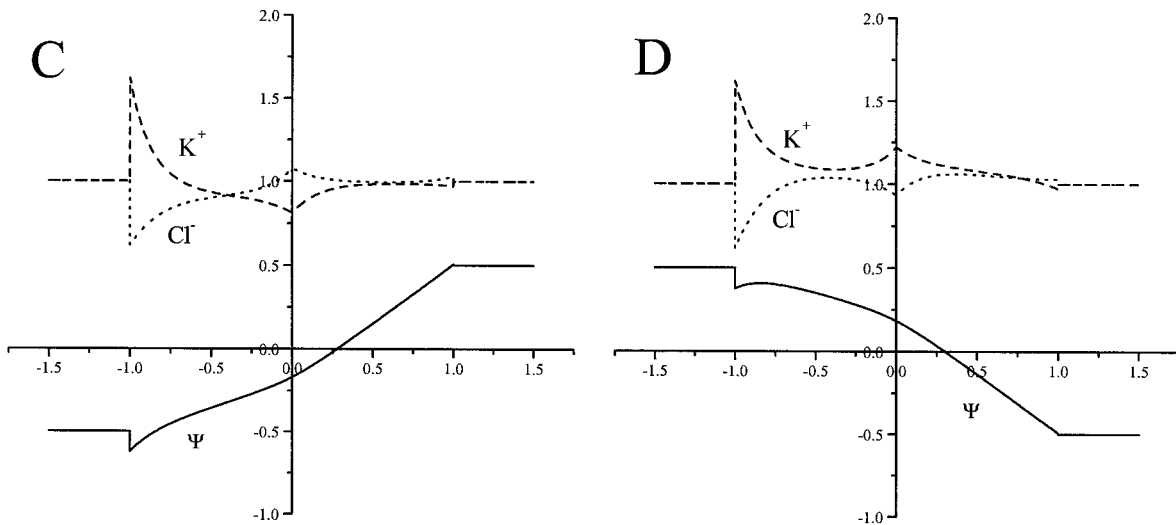# Cx26/Cx32 Variable Field/Numerical Approach

case (i)
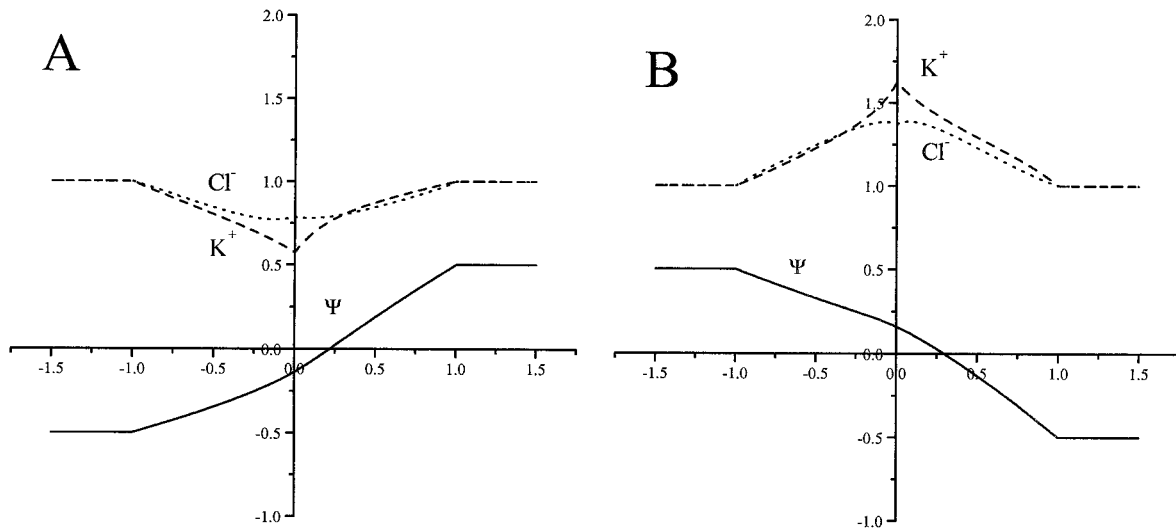
case (ii)

FIGURE 6 Microscopic picture of dimensionless ionic concentration (*upper curves in both panels*) and electrical potential profiles (*lower curves in both panels*) across the Cx26/32 heterotypic channels calculated from the numerical solution of the Nernst-Planck and Poisson equations (see Appendix) for case 1 (*A* and *B*) and case 2 (*C* and *D*). The left panels (*A* and *C*) and right panels (*B* and *D*) show parameter values when the Cx26 side is held at -100 mV and $+100$ mV relative to the Cx32 side, respectively. Potassium ion concentrations (——), chloride ion concentrations ($\cdots\cdots$), and electric potentials (——) are plotted as functions of dimensionless distance along the channel. The left (Cx26) and right (Cx32) hemichannels have mouths opening into the cellular cytoplasms at abcissa values of -1.0 and 1.0, respectively. The abrupt changes in ionic concentrations at the mouths of the channel in case 2 result from the jumps in electrical potential arising from the assumed surface potentials. All graphs show a significant bend in the electrical potential around the junction between hemichannels. In case 1 the ionic concentrations are significantly lower than bulk when the Cx26 side is negative and higher than bulk when the Cx26 side is positive with respect to the Cx32 side.

cation/anion selectivity of a channel from the unitary conductance ratios. The limitations of this approach are revealed in the work of Wang and Veenstra (1997) and Beblo and Veenstra (1997), where the homotypic rCx43 and rCx40 channels were demonstrated to have identical K^+/Cl^- permeability ratios ($P_{K/Cl}$) of 8:1, despite different R_p

FIGURE 7   Illustration depicting the differences between the electrical gradient and ionic concentration profiles predicted by the numerical solution of case 1 in the model presented in the text. Both positive (*A*) and negative (*B*) 100 mV V_j values with respect to Cx26 in a Cx26/Cx32 heterotypic channel are shown. (*I*) On initial application of the transjunctional voltage, the currents carried by anions and cations in the two hemichannels are mismatched because of the different conductances and ionic selectivities of the two hemichannels. (*II*) This can be partially alleviated by a distortion of the potential drop across the channel so that there is a lower electrical driving potential across the higher conductance hemichannel (composed of Cx26). However, this still leaves a mismatch in the fluxes so that, when the Cx26 side is positive (*A*), the influx of both anions and cations is greater than the efflux. The reverse is true when the Cx26 side is relatively negative (i.e., efflux exceeds influx; *B*). (*III*) The mismatched ionic fluxes lead to either an accumulation (*A*) or depletion (*B*) of both ions within the pore. This creates a diffusive gradient that, in case *A*, opposes influx and aids efflux, thus equalizing the currents carried by both anions and cations in each hemichannel. The reverse situation serves to equalize the currents in case *B*. The net result is that, in case *A*, the 100-mV transjunctional potential is applied across an average ionic concentration that is significantly higher than that of bulk cytoplasm. In contrast, the same potential of opposite polarity (case *B*) would be applied across an average ionic concentration in the pore that is significantly lower than in bulk cytoplasm. This generates the rectification reported for these heterotypic channels.
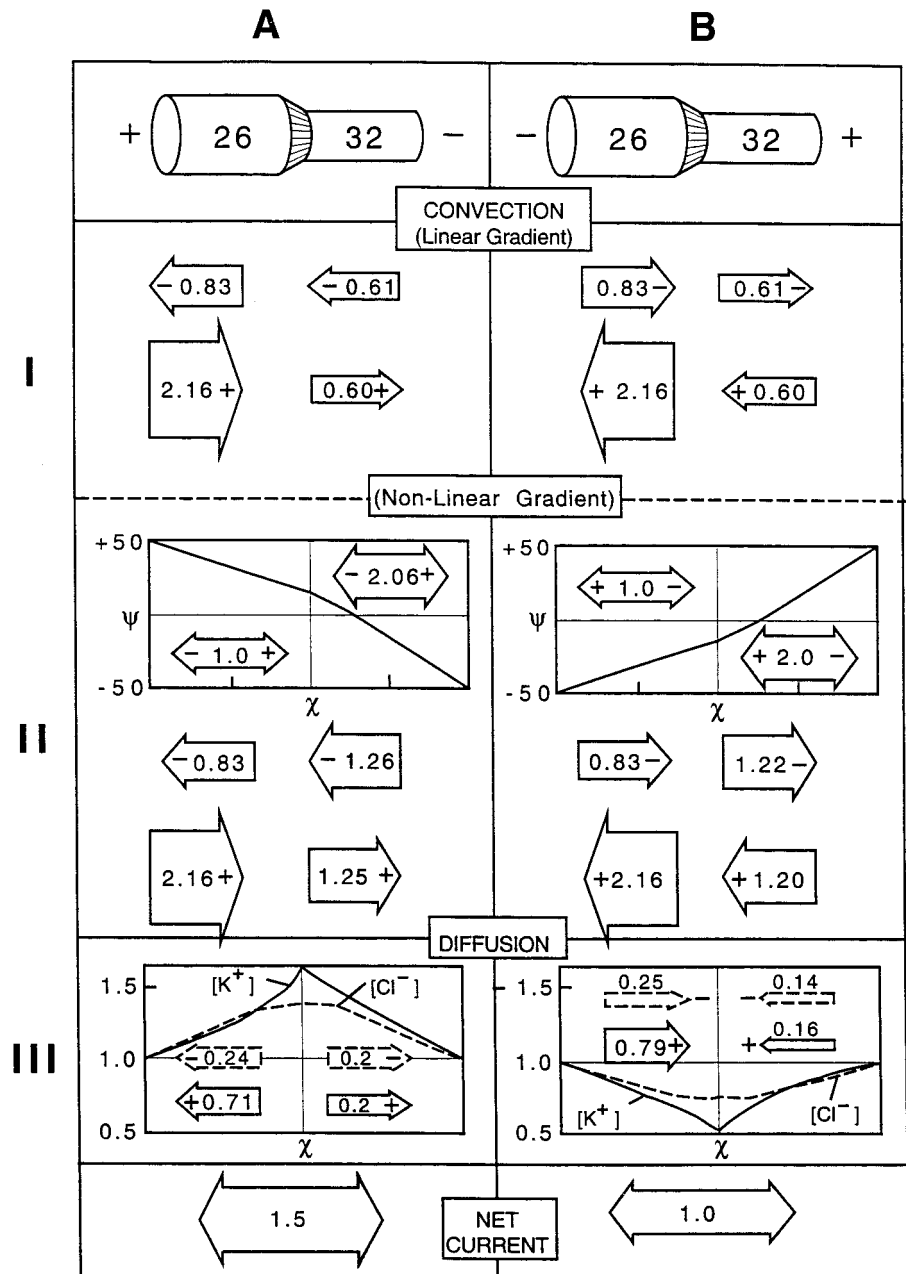
values of 0.77 for rCx43 and 0.22 for rCx40. In part, this appears to be due to the fact that relative cation:anion and anion:anoion permeability ratios can differ from those of bulk solution (an assumption inherent in estimates of R_p). The actual ionic permeabilities are likely to be quantitatively different from the results obtained from the R_p estimations. More accurate values for AP_s, determined from asymmetrical ionic reversal potential measurements (Wang and Veenstra, 1997; Beblo and Veenstra, 1997) would affect some of the parameters derived in the models presented here. However, they would not change the basic rectification that is observed. Hence, these R_p values were deemed an appropriate starting point for the modeling analyses presented, with refinement of the quantitative conclusions being readily accomplished at a future time.

The gating properties of the homotypic Cx26 and Cx32 channels and the Cx26/32 heterotypic channels expressed in the N2A cells here are indistinguishable from those reported previously in *Xenopus* oocytes (see Fig. 2), demonstrating the independence of these properties from the expression system. In agreement with the findings reported by Bukauskas et al. (1995), we demonstrated that the rectification observed at the macroscopic level was due to an increase in channel conductance as more positive V_j is applied with respect to the Cx26 side (see Fig. 4, *E* and *F*). Specifically, γ_j was found to vary linearly with V_j. The slopes and *y* intercepts of the $\partial \gamma_j / \partial V_j$ relationships in Kglutamate, Kaspartate, and KCl (data not shown) follow the same order as the aqueous mobilities of the anions. This is a unique property for an ion channel, yet the previous study offered

no biophysical mechanism underlying this phenomenon. Toward this end, we have developed, from first principles, a one-dimensional model of electromigration of small ions through the gap junctional channel that can be adapted to both homotypic and heterotypic channels.

The model is developed from the Nernst-Planck equations describing ionic concentrations within a pore and the Poisson equation describing the electrical field arising from both the applied voltage and the contribution of the ions within the pore. The basic formulation has been described previously (e.g., by Chen and Eisenberg, 1993) and applied with remarkable success to other channels such as Ca^{2+} channels (Nonner and Eisenberg, 1998). Here we have applied this model to the unique situation of two channels, each with its own properties (at least in the case of heterotypic junctions), connected in series. This provides a description of ion flux through gap junctions that both predicts the general rectifying trend observed empirically and provides insights into the underlying molecular mechanisms.

The model as presented takes a remarkably simplistic view of the channel, treating it as a somewhat featureless permeation pathway. Permeability characteristics in each hemichannel are simply derived from a combination of partitioning coefficients for each ionic species (K_s^h), reflecting the affinity of that particular ion for the pore; diffusion constants for each ionic species (D_s^h), reflecting the mobility of that ion along the length of the pore; and a surface (Donnan) potential at the cytoplasmic entrance to the hemichannel (E^h) that allows for charge-selective mouth effects. This approach seems the only reasonable one at this point, given the absence of structural information on, or energetic profiles of, the gap junction pore. Specific features can be readily incorporated into future iterations of the model as the information becomes available. In our current treatment, two extreme cases are considered wherein the demonstrated cation/anion selectivities of Cx26 and Cx32 are incorporated entirely into differences in the pore permeability parameters (defined by K_s^h and D_s^h; case 1), or entrance effects through a surface potential E^h (analogous to a Donnan potential; case 2).

Cast in a somewhat different format, Teorell (1953) had previously presented the equivalent of case 2 in terms of the effects of asymmetrical Donnan ratios (r^l and r^r) on unidirectional fluxes across a homogeneous membrane where $A^l P^l = A^r P^r$. It is valuable to compare these insights to those obtained here. He found that

$$\frac{\mu_{J_s^+}}{\sigma_{J_s^+}} = -\left(\frac{C_{bulk}^l}{C_{bulk}^r}\right)\left(\frac{r^l}{r^r}\right)\exp[(\Delta\Psi^l - \Delta\Psi^r)F/RT]$$

and

$$\frac{\mu_{J_s^-}}{\sigma_{J_s^-}} = -\left(\frac{C_{bulk}^l}{C_{bulk}^r}\right)\left(\frac{r^r}{r^l}\right)\exp[-(\Delta\Psi^l - \Delta\Psi^r)F/RT].$$

The $(r^l/r^r)^z\exp[z(\psi^l - \psi^r)F/RT]$ term was defined as the "rectification ratio." It is apparent from the derivations of

Eqs. 26a,b from Eqs. 22 and 23 that under the conditions of asymmetrical mobilities within the membrane (i.e., $A^l P^l \neq A^r P^r$), the "rectification ratio" becomes equal to $(A^l P^l/A^r P^r)(r^l/r^r)^z\exp[z(\Delta\psi^l - \Delta\psi^r)F/RT]$. In case 1, the Donnan ratios are incorporated into the $A^{26}P^{26}$ and $A^{32}P^{32}$ terms, and in case 2 they remain separate from the $A^{26}P^{26}$ and $A^{32}P^{32}$ terms, which are slightly altered in value from case 1, as all ion selectivity is attributed to the Donnan equilibrium.

Both an analytical approximation (based on a modified GHK equation) and a full numerical solution of the PNP model presented here predict rectification of heterotypic gap junction channels if formed between two connexins with different ionic selectivities, whether attributed to permeability properties of the hemichannel pore (case 1) or to Donnan ratios (r_s) describing ion entrance into the channel (case 2). Using the R_p values derived empirically from Cx26 and Cx32 homotypic channels, the predicted degree of rectification of Cx26/32 channels is significantly less than that observed empirically. Better fits at one or other polarity of V_j can be achieved with more extreme R_p values, but the overall fit to the data is not improved over that presented in Fig. 5. The inadequacies of the current model to fully predict the behavior of Cx26/Cx32 channels is not surprising, given the complete lack of knowledge of the structure of the pore, or the basis of the selectivity properties of gap junctions. In fact, as stated recently by Richard Horn in a commentary on the analogous PNP2 model of Nonner and Eisenberg (1998) applied to the Ca^{2+} channel, "the successes . . . are stunning," given the "rather featureless permeation pathway" utilized by the model. This lack of molecular detail on the pore is certain to produce inaccuracies in determining the basis for ion selective permeability. Asymmetrical salt reversal potential experiments on rCx40 and rCx43 channels suggest that at least one site of cation-anion interaction exists in each of these hemichannels (Veenstra, personal observation). Ultimately, such information can be incorporated into a full three-dimensional form of the model that can account for substructure within the pore. However, this must await higher resolution structural information on the channel itself so that the locations of fixed charges, physical constrictions (Levitt, 1991), and other selectivity filters within the pore are known and not speculated on. Further complications to this modeling would also be introduced if hemichannels do not behave independently. Currently we have assumed that hemichannels retain the properties they display in homotypic pairings, yet voltage gating properties of hemichannels have already been shown to be modified in heterotypic docking of connexins (Hennemann et al., 1992; White et al., 1995). Thus it remains possible that perm-selectivity features could be modified as well.

Despite the simplistic premise of the model presented here, it allows us to go beyond phenomenological observations by offering a plausible molecular mechanism to explain the rectifying characteristics of these heterotypic channels that does not require invoking novel gating mechanisms or specific ion binding sites in the channel. The

analytical solution we present proposes a fixed charge within the pore to maintain the constant-field assumption inherent in GHK. However, removal of this assumption still allows for a numerical solution that predicts the same degree of rectification. In short, the model predicts that the difference in permeability (i.e., selectivity and conductance) between left and right hemichannels in a heterotypic gap junction produces a mismatch in the current at the junction between them when the ionic concentrations C_s are uniform and the electric field $d\Psi/dx$ is linear, as expected at the initial application of a transjunctional voltage gradient. This mismatch is alleviated through a nonlinearity in the electric field and a nonuniformity in the concentration profile of the resident anions and cations in the pore. The resulting broad maximum or minimum in C_s that develops at the center of the channel creates a diffusive gradient that serves to equalize the differences in the electrically driven ion fluxes.

The interplay of these two different effects is summarized in Fig. 7, where the case 1 scenario is presented by way of illustration. In the case where the Cx26-expressing cell is relatively positive (Fig. 7 *A*), if the electric potential were linear across the channel, Cl$^-$ would leave the Cx26 hemichannel faster than it entered the Cx32 hemichannel. The reverse is true for K$^+$, where an even greater mismatch in the mobility of the cations between hemichannels is evident (Fig. 7 *A-I*). This creates a small separation of charge leading to a nonlinear electric potential in the whole channel (Fig. 7 *A-II*). A significant charge separation is avoided, but the influx of both cations and anions continues to exceed efflux. This causes an accumulation of ions that produces a diffusive gradient that would reduce the net influx through the more permeant hemichannel and increase net efflux through the less permeant hemichannel (Fig. 7 *A-III*). This diffusive gradient has the largest effect on the major monovalent cation currents, as this ion encounters the highest permeability change while passing from the Cx26 to the Cx32 hemichannel.

Overall, the combined effect of differential $\Delta\Psi$ in each hemichannel and the diffusive gradients of anions and cations serves to equalize the currents of anions and cations in each hemichannel. The asymmetry of the current-voltage characteristics is now readily explainable. When the left (Cx26) side is relatively positive, the average concentration of ions in the channel is higher than bulk, and thus conductance is high. When the Cx26 side is relatively negative, the average concentration in the channel is lower than bulk, and thus conductance is low. It is important to note that, while the PNP interprets ionic profiles within the pore in terms of local concentrations, ion occupancy of the pore is actually a probabilistic event (i.e., higher concentration means higher probability of an ion occupying that site). Overall, this result demonstrates that any apposition of channels of differing ionic permeability in series must produce rectification similar to that documented in this specific case, as a natural consequence of microscopic conservation principles.

It is notable that Cx32 has been the common factor in all of the documented cases of rectifying heterotypic junctions

of known composition reported to date (with Cx26—Barrio et al., 1991; with Cx46 and C50—White et al., 1995; and with Cx30—Dahl et al., 1997). Consistent with differential ion selectivities of connexins as the underlying cause of rectification in heterotypic gap junctions, Cx32 is the only connexin described to date that shows little or no preference for anions over cations (based on the R_p value reported here) or a relative selectivity for passing anionic dyes (Cao et al., 1998). This stands in direct contrast to the cation selectivity present in other connexins studied to date (Veenstra et al., 1995; Veenstra, 1996; Cao et al., 1998). Nonetheless, the modeling studies presented here would predict that any heterotypic combination of connexins that show differing ionic selectivities and conductances (even differing degrees of cation selectivity) should produce rectifying channels. There is still a minimal database on the relative ionic selectivities of gap junctions composed of different connexins (see Veenstra et al., 1994, 1995; Veenstra, 1996). Furthermore, not all of those that have been tested are derived from the same species, and it is already clear that one cannot reliably assume that homologous connexins from different species have the same selectivities (Veenstra et al., 1994). Thus few useful predictions can be made at this time regarding other heterotypic connexin combinations. Although both chickCx45 and Cx43 favor cations, they show significantly different R_p values (Veenstra et al., 1994) and thus might be expected to form rectifying heterotypic channels. Some cross-species heterotypic combinations, such as humanCx37 or ratCx26 with chick Cx45 or rat Cx40, might also be predicted to show some rectification, although to a significantly lesser degree. Data from these combinations would provide a good test of the strength of the model's predictions, but what is really needed is a significant expansion of reliable measures of ionic selectivity among the diverse family of connexins.

There is a growing recognition of the significance of connexin diversity in defining the varying roles of gap junctional coupling in biological systems. The current study describes a molecular mechanism that contributes to one of the most striking consequences of interactions between connexin isotypes—the production of rectifying communication between cells. While the degree of rectification is limited, analogous to the mild selectivity shown by gap junction channels, this may be of considerable significance for creating favored routes for the passage of labile metabolites between cells, at least when electrical gradients are in evidence. The model itself also provides novel insights into understanding ion fluxes through nonuniform pores. The PNP model has already produced valuable insights into selectivity mechanisms and behavior of other channels (e.g., Nonner and Eisenberg, 1998), the most important of which is that ion concentrations within the pore significantly influence the free energy profile. However, for most channels the PNP model is hampered, as it does not account for single-file movement of ions through the channel or the removal of the hydration shell that occurs in most ion-selective channels (although this could be accounted for by

the "excess chemical potential" term of PNP theory [see Nonner and Eisenberg, 1998]). The gap junction pore, because of its diameter, does not include these effects and thus may be the ideal candidate for application of the PNP model.

APPENDIX: DETAILS OF THE NUMERICAL CALCULATIONS

Equations 1–4, 6, and 7 are cast in a convenient dimensionless form in which all concentration fields are continuous across the junction between hemichannels. We introduce

$$x = X/L, \quad c_s^h = C_s^h/K_s^h C_{\text{bulk-s}}, \quad \psi^h = \Psi^h/V_O,$$

$$\Delta v = \Delta V/V_O, \quad e^h = E^h/V_O,$$

with $L = 5.25$ nm, $C_{\text{bulk-s}} = 120$ mM, and $V_O = 100$ mV. The first two values represent our estimate for the length of a hemichannel and the bulk concentration of KCl (s = 1 for K^+, s = 2 for Cl^-) utilized in the experiments; the last value indicates the order of magnitude of the maximum voltage drop used. In terms of these variables, the preceding equations become

$$di_s^l/dx = 0, \quad i_s^l = -[dc_s^l/dx + \alpha z_s (d\psi^l/dx) c_s^l],$$
$$-1 < x < 0,$$
$$(A1)$$
$$di_s^r/dx = 0 \quad i_s^r = -[dc_s^r/dx + \alpha z_s (d\psi^r/dx) c_s^r],$$
$$0 < x < 1,$$

$$d^2\psi^l/dx^2 = -\beta \sum_s K_s^l z_s c_s^l, \quad -1 < x < 0,$$
$$(A2)$$
$$d^2\psi^r/dx^2 = -\beta \sum_s K_s^r z_s c_s^r, \quad 0 < x < 1,$$

$$c_s^l(-1) = \exp(-\alpha z_s e^l), \quad c_s^r(1) = \exp(-\alpha z_s e^r), \quad (A3)$$

$$\psi^l(-1) = \Delta v/2 + e^l, \quad \psi^r(1) = -\Delta v/2 + e^r, \quad (A4)$$

$$c_s^l(0) = c_s^r(0), \quad (A^l P_s^l/A^r P_s^r) i_s^l(0) = i_s^r(0), \quad (A5)$$

$$\psi^l(0) = \psi^r(0), \quad d\psi^l/dx(0) = d\psi^r/dx(0), \quad (A6)$$

where

$$P_k^s = \frac{K_k^s D_k^s}{2l}$$

denotes the ionic permeability (Hodgkin and Katz, 1949; Hille, 1992). The dimensionless groups α and β appearing in Eqs. A1–A3 have the numerical values

$$\alpha = \frac{FV_o}{RT} = 3.89 \quad (A7)$$

$$\beta = \frac{FL^2 C_{\text{bulk-s}}}{\epsilon V_o} = 4.59; \quad (A8)$$

the former was computed at room temperature and the latter is based on the dielectric constant of bulk water. The total dimensional voltage drop across

the channel is $V_o \Delta v$. The dimensional current in each hemichannel carried by ionic species s is given by

$$I_s^h = 2FC_{\text{bulk-s}} z_s (A^h P_s^h) i_s^h, \quad (A9)$$

and the total electric current I_s^h is just the sum $\sum_s I_s^h$. The ratios $A^l P_s^l/A^r P_s^r$ of area times permeability of left to right hemichannels and the electrostatic surface potentials E^l and E^r play a key role in determining the concentration and electric potential profiles and thereby the current-voltage characteristics of the whole channel (see Eqs. A4 and A5). Equations A1–A6 are coupled and generally inaccessible to analytical solution; in particular, calculation of the ionic concentrations requires knowledge of the electric potential, which in turn is influenced by the concentrations of ionic species in the pore (cf. Chen and Eisenberg, 1993). We have therefore developed a general numerical approximation to the solution of Eqs. A1–A6 via the method of finite differences. Upon introducing as unknowns the values of the ionic concentrations c_s^l and c_s^r, and the electric potential ψ^l and ψ^l, at $2N + 1$ discrete node points $x_{-N} = -1$, $x_{-N+1} = -(N - 1)/N$, ..., $x_{N-1} = (N - 1)/N$, $x_N = 1$, and approximating derivatives using central or one-sided finite-difference formulas accurate to $O(1/N^2)$ as appropriate, we arrive at a system of $6N + 3$ coupled nonlinear algebraic equations. (The values $c_1^l(0) = c_1^r(0)$, $c_2^l(0) = c_2^r(0)$, and $\psi^l(0) = \psi^r(0)$ collectively represent only three unknowns, as all dimensionless dependent variables are continuous across the junction between hemichannels.) These equations are solved by Newton iteration for various values of the voltage drop Δv. Satisfactory accuracy is obtained with $N = 100$. The total current can be computed via finite difference approximation at any node point (say $x_{-N} = -1$ for definiteness), because it must turn out to be independent of x.

REFERENCES

Barrio, L. C., T. M. Suchyna, T. Bargiello, L. X. Xu, R. S. Roginski, M. V. L. Bennett, and B. J. Nicholson. 1991. Gap junctions formed by connexins 26 and 32 alone and in combination are differently affected by applied voltage. *Proc. Natl. Acad. Sci. USA.* 88:8410–8414.

Beblo, D. A., and R. D. Veenstra. 1997. Monovalent cation permeation through the connexin40 gap junction channel: Cs, Rb, K, Na, Li, TEA, TMA, TBA and effects of anions Br, Cl, F, acetate, aspartate, glutamate, and NO$_3$. *J. Gen. Physiol.* 109:509–522.

Bevans, C. G., M. Kordel, S. K. Rhee, and A. L. Harris. 1998. Isoform composition of connexin channels determines selectivity among second messengers and uncharged molecules. *J. Biol. Chem.* 273:2808–2816.

Brink, P. R., K. Cronin, K. Banach, E. Peterson, E. M. Westphale, K. H. Seul, S. V. Ramanan, and E. C. Beyer. 1997. Evidence for heteromeric gap junction channels formed from rat connexin43 and human connexin37. *Am. J. Physiol.* 273:C1386–1396.

Brink, P. R., and M. M. Dewey. 1980. Evidence for fixed charge in the nexus. *Nature.* 285:101–102.

Bruzzone, R., T. W. White, and D. L. Paul. 1996. Connections with connexins: the molecular basis of direct intercellular signalling. *Eur. J. Biochem.* 238:1–27.

Bukauskas, F. F., C. Elfgang, K. Willecke, and R. Weingart. 1995. Heterotypic gap junction channels (connexin26-connexin32) violate the paradigm of unitary conductance. *Pflugers Arch. Eur. J. Physiol.* 429: 870–872.

Cao, F., R. Eckert, C. Elfgang, J. M. Nitsche, S. Snyder, D. F. Hulser, K. Willecke, and B. J. Nicholson. 1998. A quantitative analysis of con-

nexin-specific permeability differences of gap junctions expressed in HeLa transfectants and *Xenopus* oocytes. *J. Cell Sci.* 111:31–43.

Chen, D. P., V. Barcilon, and R. S. Eisenberg. 1992. Constant fields and constant gradients in open ionic channels. *Biophys. J.* 61:1372–1393.

Chen, D. P., and R. S. Eisenberg. 1993. Flux, coupling, and selectivity in ionic channels of one conformation. *Biophys. J.* 65:727–746.

Dahl, E., D. Manthey, Y. Chen, J. Schwartz, Y. S. Chang, P. A. Lalley, B. J. Nicholson, and K. Willecke. 1996. Mouse Cx30: molecular cloning and functional expression of a gap junction gene highly expressed in adult brain and skin. *J. Biol. Chem.* 271:17903–17910.

Dunlap, K., K. Takeda, and P. Brehm. 1987. Activation of a calcium-dependent photoprotein by chemical signaling through gap junctions. *Nature.* 325:60–62.

Eisenberg, R. S. 1996. Computing the field in proteins and channels. *J. Membr. Biol.* 150:1–25.

Elfgang, C., R. Eckert, H. Lichtenberg-Frate, A. Butterweck, O. Traub, R. A. Klein, D. F. Hulser, and K. Willecke. 1995. Specific permeability and selective formation of gap junction channels in connexin-transfected HeLa cells. *J. Cell. Biol.* 129:805–817.

Falk, M., L. Buehler, N. Kumar, and N. Gilula. 1997. Cell-free synthesis and assembly of connexins into functional gap junction membrane channels. *EMBO J.* 16:2703–2716.

Flagg-Newton, J., G. Dahl, and W. R. Loewenstein. 1981. Cell junction and cyclic AMP. I. Upregulation of junctional membrane permeability and junctional membrane particles by administration of cyclic nucleotide or phosphodiesterase inhibitor. *J. Membr. Biol.* 63:105–121.

Frankenhaeuser, B. 1960. Sodium permeability in toad nerve and in squid nerve. *J. Physiol. (Lond.).* 152:159–166.

Fulbridge, R. C., S. M. Fine, E. R. Unanue, and D. D. Chaplin. 1988. Expression of membrane interleukin 1 by fibroblasts transfected with murine prointerleukin 1α cDNA. *Proc. Natl. Acad. Sci. USA.* 85:5649–5653.

Goldman, D. E. 1943. Potential, impedance and rectification in membranes. *J. Gen. Physiol.* 27:37–60.

Harris, A., A. Walter, D. Paul, D. Goodenough, and J. Zimmerberg. 1992. Ion channels in single bilayers induced by rat connexin 32. *Brain Res. Mol. Brain Res.* 15:269–280.

Hennemann, H., T. M. Suchyna, H. Lichtenberg-Frate, S. Jungbluth, E. Dahl, J. Schwarz, B. J. Nicholson, and K. Willecke. 1992. Molecular cloning and functional expression of mouse connexin40, a second gap junction gene preferentially expressed in lung. *J. Cell Biol.* 117:1299–1310.

Hiemenz, P. C. 1986. Principles of Colliod and Surface Chemistry, 2nd ed. Marcel Dekker, New York.

Hille, B. 1992. Selective permeability: independence. *In* Ionic Channels of Excitable Membranes, 2nd Ed. Sinauer Associates, Sunderland, MA. 348–361.

Hodgkin, A. L., and B. Katz. 1949. The effect of sodium ions on the electrical activity of the giant axon of the squid. *J. Physiol. (Lond.).* 108:37–77.

Horan, P. K., M. J. Melnicoff, B. D. Jensen, and S. E. Slezak. 1990. Fluorescent cell labeling for in vivo and in vitro tracking. *Methods Enzymol.* 33:469–490.

Horn, R. 1998. Run, don't hop, through the nearest calcium channel. *Biophys. J.* 75:1142–1143.

Jaslove, S., and P. R. Brink. 1986. The mechanism of rectification at the electronic motor synapse of the crayfish. *Nature.* 232:63–65.

Jiang, J. X., and D. A. Goodenough. 1996. Heterotypic connexons in lens gap junction channels. *Proc. Natl. Acad. Sci. USA.* 93:1287–1291.

Kumar, N. M., and N. B. Gilula. 1996. The gap junction communication channel. *Cell.* 84:381–388.

Levitt, D. G. 1991. General continuum theory for multi-ion channels. II. Application to acetylcholine channel. *Biophys. J.* 59:278–288.

Makowski, L., D. L. Casper, W. C. Philips, and D. A. Goodenough. 1984. Gap junction structures. V. Structural chemistry inferred from x-ray diffraction measurements on sucrose sucrose accessibility and trypsin susceptibility. *J. Mol. Biol.* 174:449–481.

Moreno, A. P., B. Eghbali, and D. C. Spray. 1991. Connexin32 gap junction channels in stably transfected cells: unitary conductance. *Biophys. J.* 60:1254–1266.

Nevue, M. J., J. R. Hully, K. L. Babcock, E. L. Hertzberg, B. J. Nicholson, D. L. Paul, and H. C. Pitot. 1994. Multiple mechanisms are responsible for altered expression of gap junction genes during oncogenesis in rat liver. *J. Cell Sci.* 107:83–95.

Nicholson, B. J., R. Dermietzel, D. Teplow, O. Traub, K. Willecke, and J. P. Revel. 1987. Two homologous proteins of hepatic gap junctions. *Nature.* 329:732–734.

Nicholson, B. J., T. M. Suchyna, L. X. Xu, P. Hammernick, F. L. Cao, C. Fourtner, L. Barrio, and M. V. L. Bennett. 1993. Divergent properties of different connexins expressed in *Xenopus* oocytes. *In* Progress in Cell Research: Gap Junctions, Vol. 3. J. E. Hall, G. A. Zampighi, and R. M. Davis, editors. Elsevier Science Publishers, New York. 3–13.

Nonner, W., and R. S. Eisenberg. 1998. Ion permeation and glutamate residues linked by Poisson-Nernst-Planck theory in L-type calcium channels. *Biophys. J.* 75:1287–1305.

Paul, D. L. 1986. Molecular cloning of cDNA for rat liver gap junction protein. *J. Cell Biol.* 103:123–134.

Reed, K. E., E. M. Westpale, D. M. Larson, H.-Z. Wang, R. D. Veenstra, and E. C. Beyers. 1993. Molecular cloning and functional expression of human connexin37, an endothelial cell gap junction protein. *J. Clin. Invest.* 91:997–1004.

Saez, J. C., J. A. Connor, D. C. Spray, and M. V. L. Bennett. 1989. Hrpstocyte gap junctions are permeable to the second messenger, inositol 1:4,5-triphosphate, and to calcium ions. *Proc. Natl. Acad. Sci. USA.* 86:2708–2712.

Schwarzmann, G., H. Wiegandt, B. Rose, A. Zimmermann, D. Ben-Haim, and W. R. Loewenstein. 1981. Diameter of a cell-cell junctional membrane channel as probed with neutral molecules. *Science.* 213:551–553.

Spray, D. C., A. L. Harris, and M. V. L. Bennett. 1979. Equilibrium properties of a voltage-dependent junctional conductance. *J. Gen. Physiol.* 77:77–93.

Stauffer, K. A. 1995. The gap junction proteins β_1-connexin (Cx32) and β_2-connexin (Cx26) can form heteromeric hemichannels. *J. Biol. Chem.* 270:6768–6772.

Steinberg, T. H., R. Civitelli, S. T. Geist, A. J. Robertson, E. Hick, R. D. Veenstra, H.-Z. Wang, P. M. Marlow, E. M. Westphale, J. Laing, and E. C. Beyer. 1994. Connexin43 and connexin45 form gap junctions with different molecular permeabilities in osteoclastic cells. *EMBO J.* 4:744–750.

Teorell, T. 1953. Transport processes and electrical phenomena in ionic membranes. *Prog. Biophys.* 3:305–369.

Traub, O., J. Look, R. Dermietzel, F. Brunner, D. Hulser, and K. Willecke. 1989. Comparative characterization of the 21 kD and 26 kD gap junction proteins in murine liver and cultured mouse hepatocytes. *J. Cell Biol.* 108:1039–1051.

Tsien, R. W., and R. Weingart. 1976. Ionotropic effect of cyclic AMP in calf ventricular muscle studied by a cut end method. *J. Physiol. (Lond.).* 260:117–141.

Veenstra, R. D. 1996. Size and selectivity of gap junction channels formed from different connexins. *J. Bioenerg. Biomembr.* 28:327–337.

Veenstra, R. D., and P. R. Brink. 1992. Patch clamp analysis of gap junctional currents. *In* Cell-Cell Interactions: A Practical Approach. B. Stevenson, D. L. Paul, and W. Gallin, editors. IRL Press, Oxford. 167–201.

Veenstra, R. D., H. Z. Wang, D. A. Beblo, M. G. Chilton, A. L. Harris, E. C. Beyer, and P. R. Brink. 1995. Selectivity of connexin-specific gap junctions does not correlate with channel conductance. *Circ. Res.* 77:1156–1165.

Veenstra, R. D., H. Z. Wang, E. C. Beyer, S. V. Ramanan, and P. R. Brink. 1994. Connexin37 forms high conductance gap junctions channels with subconductance state activity and selective dye and ionic permeabilities. *Biophys. J.* 66:1915–1928.

Verselis, R. D., and P. R. Brink. 1986. The gap junction channel. Its aqueous nature as indicated by deuterium oxide effects. *Biophys. J.* 50:1003–1008.

Verselis, V. K., C. S. Ginter, and T. A. Bargiello. 1994. Opposite voltage gating polarities of two closely related connexins. *Nature.* 368:348–351.

Wang, H.-Z., and R. D. Veenstra. 1997. Monovalent cation and anion selectivity sequences of the rat connexin43 gap junction channel. *J. Gen. Physiol.* 109:491–507.

White, T. M., R. Bruzzone, D. A. Goodenough, and D. L. Paul. 1992. Mouse Cx50, a functional member of the connexin family of gap junction proteins, is lens fiber protein MP70. *Mol. Biol. Cell.* 3:711–720.

White, T. W., D. L. Paul, D. A. Goodenough, and R. Bruzzone. 1995. Functional analysis of selective interactions among rodent connexins. *Mol. Biol. Cell.* 6:459–470.

Yeager, M., and B. J. Nicholson. 1996. Structure of gap junction intercellular channels. *Curr. Opin. Struct. Cell Biol.* 6:183–192.

Zhang, J. T., and B. J. Nicholson. 1994. The topological structure of connexin 26 and its distribution compared to connexin 32 in hepatic gap junctions. *J. Membr. Biol.* 139:15–29.